Elsevier Editorial System(tm) for Fuel
Manuscript Draft

Manuscript Number: JFUE-D-16-01365R1

Title: Chemical kinetics and CFD analysis of supercharged micro-pilot ignited dual-fuel engine combustion of syngas

Article Type: Research paper

Keywords: Dual-fuel engine, Syngas combustion, Chemical kinetics, DARS, CFD simulation

Corresponding Author: Dr. Ulugbek Azimov, PhD

Corresponding Author's Institution: University of Northumbria

First Author: Nearchos Stylianidis

Order of Authors: Nearchos Stylianidis; Ulugbek Azimov, PhD; Alireza Maheri, PhD; Nobuyuki Kawahara; Eiji Tomita

Abstract: A comprehensive chemical kinetics and computational fluid-dynamics (CFD) analysis were performed to evaluate the combustion of syngas derived from biomass and coke-oven solid feedstock in a micro-pilot ignited supercharged dual-fuel engine under lean conditions. The developed syngas chemical kinetics mechanism was validated by comparing ignition delay, in-cylinder pressure, temperature and laminar flame speed predictions against corresponding experimental and simulated data obtained by using the most commonly used chemical kinetics mechanisms developed by other authors. Sensitivity analysis showed that reactivity of syngas mixtures was found to be governed by H2 and CO chemistry for hydrogen concentrations lower than 50% and mostly by H2 chemistry for hydrogen concentrations higher than 50%. In the mechanism validation, particular emphasis is placed on predicting the combustion under high pressure conditions. For high hydrogen concentration in syngas under high pressure, the reactions HO2+HO2=H2O2+O2 and H2O2+H=H2+HO2 were found to play important role in in-cylinder combustion and heat production. The rate constants for H2O2+H=H2+HO2 reaction showed strong sensitivity to high-pressure ignition times and has considerable uncertainty. Developed mechanism was used in CFD analysis to predict in-cylinder combustion of syngas and results were compared with experimental data. Crank angle-resolved spatial distribution of in-cylinder spray and combustion temperature was obtained. The constructed mechanism showed the closest prediction of combustion for both biomass and coke-oven syngas in a micro-pilot ignited supercharged dual-fuel engine.

Highlights (for review)

- CFD-compatible syngas chemical kinetics mechanism has been developed for micro-pilot ignited supercharged dual-fuel engine combustion.
- The new mechanism predicted in-cylinder combustion performance well for both biomass and coke-oven syngas.
- Due to the strong temperature dependence of HO2+OH=H2O+O2 reaction, two expressions of this reaction were used to accurately simulate biomass-derived syngas.
- To accurately simulate coke-oven syngas, the rate parameter for H2O2+H=H2+HO2 reaction had to be adopted from Hong et al.[49] with the adjusted power factor, with the rate which is outside of the uncertainty factor limits proposed by Konnov [42].

Chemical kinetics and CFD analysis of supercharged micro-pilot ignited dual-fuel engine combustion of syngas

Nearchos Stylianidis [1], *Ulugbek Azimov*[1*], *Alireza Maheri*[1], *Eiji Tomita*[2], *Nobuyuki Kawahara*[2]

[1]*Department of Mechanical and Construction Engineering, University of Northumbria, City campus, Newcastle upon Tyne, NE1 8ST, United Kingdom*
[2]*Department of Mechanical Engineering, Okayama University, Tsushima-Naka 3, Okayama 700-8530, Japan*

*Corresponding author:
Dr. Ulugbek Azimov
Senior Lecturer
Dept. of Mechanical and Construction Engineering
University of Northumbria
City Campus, Wynne-Jones Centre, Room 305
Newcastle upon Tyne
NE1 8ST, UK
Phone: +44 191-2437663
Email: ulugbek.azimov@northumbria.ac.uk

Dr. Alireza Maheri
Senior Lecturer
Dept. of Mechanical and Construction Engineering
University of Northumbria
City Campus, Wynne-Jones Centre, Room 201
Newcastle upon Tyne
NE1 8ST, UK
Phone: +44 191-2433860
Email: alireza.maheri@northumbria.ac.uk

Mr. Nearchos Stylianidis
PhD student
Dept. of Mechanical and Construction Engineering
University of Northumbria
City Campus, Wynne-Jones Centre, Room 209
Newcastle upon Tyne
NE1 8ST, UK
Email: nearchos.stylianidis@northumbria.ac.uk

Prof. Nobuyuki Kawahara
Dept. of Mechanical Engineering, Okayama University
3-1-1 Tsushima-naka, Kita-ku, Okayama 700-8530, JAPAN
Phone: +81-86-251-8235
FAX: +81-86-251-8266
Email: kawahara@mech.okayama-u.ac.jp

Prof. Eiji Tomita
Dept. of Mechanical Engineering, Okayama University
3-1-1 Tsushima-naka, Kita-ku, Okayama 700-8530, JAPAN
Phone: +81-86-251-8049
FAX: +81-86-251-8266
Email: tomita@mech.okayama-u.ac.jp

Nomenclature

BTDC:	Before top dead centre
ATDC:	After top dead centre
CA:	Crank angle
CI:	Compression ignition
CNG:	Compressed natural gas
IC:	Internal combustion
ROHR (J/deg):	Rate of heat release
SI:	Spark ignition
TDC:	Top dead centre
BMG:	Biomass Gasification
COG:	Coke-Oven Gasification

Chemical kinetics and CFD analysis of supercharged micro-pilot ignited dual-fuel engine combustion of syngas

Nearchos Stylianidis [1], Ulugbek Azimov[1], Alireza Maheri[1], Eiji Tomita[2], Nobuyuki Kawahara[2]*

[1]*Department of Mechanical and Construction Engineering, University of Northumbria, City campus, Newcastle upon Tyne, NE1 8ST, United Kingdom*
[2]*Department of Mechanical Engineering, Okayama University, Tsushima-Naka 3, Okayama 700-8530, Japan*

Abstract

A comprehensive chemical kinetics and computational fluid-dynamics (CFD) analysis were performed to evaluate the combustion of syngas derived from biomass and coke-oven solid feedstock in a micro-pilot ignited supercharged dual-fuel engine under lean conditions. The developed syngas chemical kinetics mechanism was validated by comparing ignition delay, in-cylinder pressure, temperature and laminar flame speed predictions against corresponding experimental and simulated data obtained by using the most commonly used chemical kinetics mechanisms developed by other authors. Sensitivity analysis showed that reactivity of syngas mixtures was found to be governed by H_2 and CO chemistry for hydrogen concentrations lower than 50% and mostly by H_2 chemistry for hydrogen concentrations higher than 50%. In the mechanism validation, particular emphasis is placed on predicting the combustion under high pressure conditions. For high hydrogen concentration in syngas under high pressure, the reactions $HO_2+HO_2=H_2O_2+O_2$ and $H_2O_2+H=H_2+HO_2$ were found to play important role in in-cylinder combustion and heat production. The rate constants for $H_2O_2+H=H_2+HO_2$ reaction showed strong sensitivity to high-pressure ignition times and has considerable uncertainty. Developed mechanism was used in CFD analysis to predict in-cylinder combustion of syngas and results were compared with experimental data. Crank angle-resolved spatial distribution of in-cylinder spray and combustion temperature was obtained. The constructed mechanism showed the closest prediction of combustion for both biomass and coke-oven syngas in a micro-pilot ignited supercharged dual-fuel engine.

Keywords: Dual-fuel engine, Syngas combustion, Chemical kinetics, DARS, CFD simulation

1. Introduction

Advanced reciprocating engines are considered a potential means of converting syngas into power because of their role in distributed energy production and their combination of high efficiency and low cost [1]. Syngas consists of combustible gases composed of mainly carbon monoxide (CO), hydrogen (H_2), and methane (CH_4), and non-combustible gases composed of mainly nitrogen (N_2) and carbon dioxide (CO_2). Varying proportions of H_2, CO, CH_4, CO_2, H_2O, and N_2 may be present [2]. Mixtures of H_2 and CO have high antiknock behaviour and therefore could serve as fuels for internal combustion engines [3, 4]. However, the addition of hydrogen to carbon monoxide or methane tends to increase combustion temperatures and NOx emissions under stoichiometric conditions [5]. Therefore, such mixtures are more appropriate for lean-burn applications, where combustion temperatures are moderated by excess air.

The main benefit of utilizing syngas as a fuel for power generation is obtained when syngas is used in dual-fuel engines that operate under compression ignition with a lean mixture, using a pilot injection of diesel fuel [8]. Some fuels do not have sufficient ignition properties to enable ignition, so two fuels must be used. The ignition of the primary fuel (typically gaseous) is activated by the in-cylinder conditions. In this case, first, a pilot diesel fuel is injected, resulting in ignition and a subsequent temperature rise in the combustion chamber [7, 8]. Then, the primary gaseous fuel, which in this case is syngas, is ignited as the chamber temperature increases, with subsequent combustion. Dual-fuel engines have been employed for a wide range of applications to utilize gaseous fuels. They are most commonly modified diesel engines and can achieve very low emission levels, particularly for smoke and particulates. The benefits of the dual-fuel conversion, if compared to the conventional diesel engine operation, include high efficiency, fuel flexibility, smoother and quieter operation, significantly longer engine life between overhauls, fuel savings, and enhanced safety.

A few published works have described the use of syngas as a fuel for internal combustion (IC) engines. These include the work of Karim and coworkers [9, 10], McMillian and Lawson [11], Christodoulou and Megaritis [12]. Bilcan [13] studied the use of various gaseous fuels, including syngas, in dual-fuel engines.

Baratieri *et al.* [14] conducted a comparative analysis on the use of biomass-based syngas in internal-combustion (IC) engines and combined-cycle gas turbine (CCGT) plants. They concluded that the IC engine configuration is characterized by a significant thermal energy fraction that makes it possible to reach global energy efficiencies higher than 70%. Boehman and Le Corre [15] surveyed the published work on syngas combustion in reciprocating engines and focused on dual-fuel combustion in compression-ignition engines. Tomita *et al.* [16] investigated the combustion characteristics and performance of supercharged syngas with micro-pilot ignition in a dual-fuel engine. With a certain increase in syngas hydrogen content, the engine was found to operate with stable combustion and high efficiency, even at an equivalence ratio of 0.45, because the increased hydrogen content enhanced the lean limit of the mixture. Roy *et al.* [17, 18] studied the effect of hydrogen content in the syngas produced from biomass and the effect of exhaust gas recirculation (EGR) in the syngas produced from hydrogen-rich coke oven gas on the performance and exhaust emissions of a dual-fuel engine. They found that the engine power with the high-H_2-content syngas increased by 12%, and that the high-H_2-content syngas was superior to the low-H_2-content gas for leaner operations.

Because the composition of syngas depends on the solid feedstock and its gasification process, it is very difficult to model and predict engine in-cylinder syngas combustion. A universal CFD-compatible syngas chemical kinetics mechanism must be developed that could cover the broad range of syngas composition and engine combustion conditions. While developing syngas mechanism usually H_2/CO structure is considered, however some syngas types derived from biomass and coke-oven solid feedstock may also include CH_4, as shown in this paper. Another complexity rises due to the effect of in-cylinder turbulence on combustion.

Improvements made to the fuel flexibility of syngas-combustion technology by optimizing the combustion mechanism will provide for an increased acceptable range in the variation of fuel composition and conditions. Several research groups have developed chemical kinetics mechanisms to simulate syngas combustion. Yetter *et al.* [19] developed a comprehensive reaction mechanism for CO and H_2, which are considered the main combustible species in syngas. Saxena and Williams [20] tested a small detailed chemical kinetic

mechanism for the combustion of hydrogen and carbon monoxide. They made a few revisions to the rate parameters for the elementary steps in the mechanism for hydrogen [21–24], deleted the hydrogen initiation step, and added an initiation step for CO along with changes to the three-body recombination rates and chaperon efficiencies. They reported that with these changes, a reasonable agreement was obtained with measured burning velocities, diffusion-flame extinction conditions, and autoignition times. Frassoldati *et al.* [25, 26] studied the combustion and flame structure of CO–H_2 mixtures. They developed a kinetic scheme for turbulent diffusion flames by coupling a kinetic postprocessor with a computational fluid dynamics (CFD) code to investigate the flame structure and pollutant formation. Slavinskaya *et al.* [27] developed a skeletal reaction mechanism for syngas combustion in gas turbines with 12 species and 20 irreversible reactions. This mechanism was validated for pressures up to 20 bar with different mixture contents and fuel–air ratios. Starik *et al.* [28] developed a kinetic model that describes the processes of ignition and combustion of CO–H_2–O_2–N_2 mixtures. The model was validated over wide ranges of temperature, pressure, and equivalence ratio using experimental data for the ignition delay time and laminar-flame propagation velocity, and also for the evolution of the most important species. Sun *et al.* [29] studied high-pressure flame speeds and performed kinetic modelling of CO/H_2 combustion. The comparison between the modelled results and laboratory measurements suggested that the accuracy of the thermochemical data and the elementary rate constants is crucial for obtaining satisfactory performance of the reaction mechanism. Sivaramakrishnan *et al.* [30] studied the combustion of CO/H_2 mixtures at elevated pressures. They showed that the model they developed underpredicted CO and O_2 decay and CO_2 formation at very high pressures of 256 and 450 bars. They concluded that HO_2 radical reactions appear to be among the most sensitive reactions in the model under these conditions. Cavaliere *et al.* [31] modelled kinetically the ignition of syngas/air mixtures at low temperature and high pressure with the four reaction mechanisms described by Frassoldati *et al.* [25], Saxena and Williams [20], Yetter *et al.* [19], and GRI Mech 3.0 [32]. They found that for a mixture of CO and H_2, all mechanisms predicted the experimental data accurately for temperatures above 1000 K regardless of the pressure. But

195 below this temperature, the simulation results deviated from the experimental data. Mittal *et al.* [33] used
196 experiments with a rapid-compression machine and numerical studies to evaluate the combustion mechanism
197 for CO/H_2 mixtures at high pressures in the range of 15–50 bar and at temperatures of 950–1100 K. Their
198 results demonstrated that any evaluation of a kinetic scheme by reference to ignition delays must be treated
199 with some caution when the kinetic uncertainties are not taken into account. Chaos and Dryer [34] reviewed
200 the possibility of using gas turbine syngas combustion with higher pressures and lower temperatures to test the
201 comprehensive nature of the existing detailed chemical kinetic models. They proposed kinetic changes to
202 improve the predictions of syngas combustion under these conditions and emphasized that the higher-pressure,
203 lower-temperature conditions encountered in gas turbines point to the importance of and the need for further
204 theoretical as well as experimental studies of elementary reactions involving HO_2 and H_2O_2 chemistry.
205 Keromnes et al. [35] performed detailed chemical kinetic modelling study of hydrogen and syngas
206 mixtures at elevated pressures and presented new oxidation data. The mechanism accurately reproduces
207 high-pressure and intermediate- to high-temperature data relevant to gas turbine conditions. They showed that
208 syngas chemistry is governed by the hydrogen chemistry, and CO addition has an inhibiting effect. The
209 predictions of the mechanism for a series of fundamental shock tube, RCM, and flame speed experiments are
210 in good agreement. However, some differences appear at low to intermediate temperatures due to the
211 importance of the oxidation pathway through reactions $H+O_2(+M)=HO_2(+M)$, $H_2O_2(+M)=OH+OH(+M)$ and
212 $H_2O_2+H=H_2+HO_2$.
213 Lee et al. [36] performed comprehensive comparison of chemical kinetics mechanisms for syngas/biogas
214 mixtures. They found that NUIG2013 mechanism [37] was in closest agreement with the measured ignition
215 delay and laminar flame speed for the investigated mixtures. However, there are several mixture compositions
216 and conditions for which the NUIG2013 mechanism fails to accurately predict the ignition delay time results.
217 These include syngas mixtures with CH_4 gas content, and CH_4/H_2 mixtures at low hydrogen concentrations
218 ($\leq$40% H_2).

Olm et al. [38] compared 16 chemical kinetics mechanisms developed by different authors and identified well performing mechanisms and those that are only good at certain conditions for a certain types of experiments. They have concluded that three of syngas mechanisms, Keromnes-2013 [35], NUIG-NGM-2010 [39] and Li-2007 [40] showed closest match with experiments, while others may only excel in certain categories and are not able to provide general reliability across the various types of experiments.

The syngas mechanisms described above were mainly developed under the conditions which excluded the effect of turbulence and they are not able to accurately represent the interactions between turbulent fluid dynamics and chemical kinetics in an IC engine cylinder. These turbulence–chemistry interactions can have significant effects on ignition delay, flame stability and pollutant formation during engine combustion. There is an urgent need for a reliable engine-simulation model that represents the turbulence–chemistry interactions by combining CFD and a syngas chemical kinetics. It has been shown that the effects of turbulent mixing must be considered to obtain better agreement with experiments during the combustion phase [41]. In earlier studies we made an attempt to analyse dual-fuel engine combustion with syngas and developed a syngas chemical kinetics mechanism. In this work the important hydrogen-based reaction rates proposed by Keromnes et al. [35] and Konnov [42] were included into mechanism and comprehensive study was performed to develop IC engine-compatible syngas chemical kinetics mechanism and validate against engine experiments. This model will help predict the combustion behaviour of syngas with various chemical compositions from different feedstock, such as biomass, coal, and refinery residues, as a necessary precondition for establishing numerical tools to verify system designs at early developmental stages.

2. Numerical and experimental setup

In this study, two types of combustion analysis were performed. First, a zero-dimensional chemical kinetic analysis was performed using the Digital Analysis of Reaction Systems (DARS) [43]. DARS has been built with the specific purpose of enabling detailed chemical kinetics analysis to engineering applications, with one

particular focus on internal combustion engines. It handles gas phase chemistry via a suite of reactor models and reaction mechanisms. For this work we used a single-zone model for homogeneous-charge compression-ignition (HCCI), rapid compression machine (RCM) model and free propagating flame model. This analysis was performed to compare a new syngas chemical kinetics mechanism with existing mechanisms and validated against the experiments performed with constant volume reactor, shock tube and RCM. Several characteristics of syngas combustion were compared, such as, ignition delay, flame propagation, in-cylinder pressure and temperature. For DARS HCCI analysis the intake-valve closure (IVC) time was 135 crank-angle degrees (CA°) before top dead centre (BTDC), and the simulation was run for 265 CA°. The gas mixture pressure and temperature at IVC were 225 kPa and 450 K, respectively. DARS RCM analysis was performed at compression pressures (2-80bar) and temperatures (450-1000K). To calculate the laminar flame speed, free propagating flame model was used at pressures (1-80bar) and temperatures (298-1000K).

Second, a multidimensional CFD analysis was performed using the Star-CD V4.2 code simulating the combustion in a water-cooled four-stroke single-cylinder engine with two intake and two exhaust valves, described in detail in [17]. In this engine, the autoignition of a small quantity of diesel pilot fuel, injected into the combustion chamber before top dead centre (TDC), initiates the combustion. The burning diesel fuel then ignites the gaseous fuel. A commercial solenoid-type injector that is typically used for diesel-only operations was modified to ensure that only a small quantity of fuel was injected. The seven-hole nozzle of the commercial injector was replaced by one with four holes, 0.1 mm in diameter. The diesel-fuel injection timing and duration were controlled through signals transferred to the injector from the injector driver. A common-rail injection system was employed to supply a constant injection pressure of 80 MPa to the injector. The quantity of injected pilot diesel fuel was 1.2 mg/cycle. The simulations began from the intake valve closure at 135° CA BTDC and were carried until 130° CA after top dead centre (ATDC). The simulation conditions with the engine specifications and different types of primary gaseous fuel compositions used in this study are given in Tables 1 and 2, respectively. This version of Star-CD incorporates the CHEMKIN code to formulate the

gas-phase chemistry with an advanced solver approach. The Star-CD code provides CHEMKIN with the thermodynamic information for the computational cells, and the CHEMKIN code returns the new species information after solving the chemistry. After solutions are obtained for all cells, the mass transfer, heat transfer, and flow between cells are simulated by the corresponding sub-models. Then, the interactions between the turbulent mixing and the chemical reactions are implemented. The CFD model was based on the Reynolds-averaged governing equations; it was set to account for turbulence, the liquid fuel-injection spray, and chemical mechanisms and was used the experimental conditions. The standard high-Reynolds number k–ε model was used for the turbulence modelling. A constant temperature of 450 K was used for the cylinder wall and cylinder head, and 500 K was used for the piston surface. The pressure-implicit split-operator (PISO) algorithm was used to simulate the transient flow of the engine. The injection process included the flow in the nozzle hole and the atomisation process. The properties of atomisation and secondary break-up were calculated by the Reitz–Diwakar model [44, 45]. To reduce the computation time, a 90° moving-sector mesh of 13,256 cells with cyclic boundaries was used to represent a bowl-in-piston configuration that was representative of the experimental single-cylinder pilot-ignited dual-fuel engine [17]. A grid size between 0.5 and 2.0 mm and a time step of 0.1° CA provided good numerical accuracies and computation stabilities. The sensitivity of the grid was validated by comparing the motoring in-cylinder pressure histories from experiments.

3. Development of the syngas kinetics mechanism

Because the composition of syngas depends on the solid feedstock and its gasification process, it is very challenging to develop a universal CFD-compatible syngas chemical kinetics mechanism that could cover the broad range of engine combustion conditions. While developing syngas mechanism usually H_2/CO structure is considered, however some syngas types derived from biomass and coke-oven solid feedstock may also include CH_4, as shown in this paper. Another complexity rises due to the effect of turbulence on combustion. Previous studies showed that chemical kinetics mechanism with Chemkin models cannot accurately simulate engine

292 in-cylinder combustion and the effect of turbulence must be considered [41].

293 Therefore, for this research we have developed a CFD-compatible syngas chemical kinetics mechanism,
294 shown in Table 3, which can simulate dual-fuel engine combustion at various engine conditions, as shown in
295 Tables 1 and 2. The mechanism was compared with H_2/CO syngas mechanisms developed and validated
296 against experiments by other authors {Keromnes et.al. [35], Frassoldatti et al. [25] and GRI Mech 3.0 [32]}.
297 To consider CH_4 component in the syngas composition, the nine-step reduced mechanism for CH_4
298 autoignition by Li *et al.* [46] was used to add methane chemistry to H_2/CO reactions. To simulate the
299 pilot-injected diesel spray and ignition, the chemistry of C_7H_{16} was included in the constructed mechanisms
300 as a single-step reaction, $C_7H_{16} + 11O_2 = 7CO_2 + 8H_2O$, based on an eddy breakup (EBU) mixing
301 representation by specifying the EBU reaction parameters [47]. Previous studies have shown that for
302 conventional diesel combustion, both diesel and C_7H_{16} fuels show a similar ROHR [48]. This implies that
303 C_7H_{16} is only used to initiate the pilot ignition of syngas. After the syngas is ignited, the combustion proceeds
304 without any C_7H_{16} chemistry. The reason for this simplification is that the amount of injected diesel fuel was
305 1.2 mg/cycle, which provides only 2% of the total energy value in the cylinder, with negligible contribution to
306 the total ROHR. Previous results [17, 18] have shown that when micro-pilot injection is used, the ROHR
307 profiles do not include any changes due to the pilot diesel fuel combustion, which is opposite to what has
308 been found when the amount of pilot-injected fuel is high, as in [15]. Additionally, the experimental results
309 showed an undetectable level of soot formation during micro-pilot diesel fuel combustion.

310

311 *3.1 Sensitivity analysis*

312 A sensitivity analysis was performed for syngas Type 1 at temperature 1000K, equivalence ratio 0.63 and
313 pressure 10, 30 and 50 bar. In DARS, the sensitivity analysis is a representation of a simultaneous reaction
314 flow. Sensitivities are transported through the mechanism in the sense that a species is rated according to its
315 own importance and its involvement in producing or consuming important species [43]. The species

sensitivity, defined for each species, represents the sensitivity towards a chosen parameter *A*, and is the sum of the reaction sensitivities in which the species participate:

$$S_{A,i}^{S} = \left| \sum_{k=1}^{N_r} \frac{\partial \psi_A}{\partial r_k} \cdot \frac{v'_{i,k}}{c_i} r_k \right| \quad (1)$$

Here $S_{A,i}^{S}$ contains the information on how sensitive an arbitrary parameter *A* in the vector of unknowns, $\partial \psi_A$, is to species *i*.

From sensitivity analysis the main hydrogen- and carbon-based reactions that play a key role were identified as shown in Figure 1. The importance of these reactions was also highlighted by other research groups [35, 42, 49]. This analysis shows that $H_2O_2(+M)=OH+OH(+M)$, $H_2O_2+H=H_2+HO_2$ and $CO+H_2O=CO_2+H_2$ reactions contribute to the increasing reactivity of the mixture and $H_2+O=OH+H$, $O_2+CO=CO_2+O$ and $CH_4+OH=CH_3+H_2O$ reactions contribute to the decreasing reactivity. A brief description of importance of each of these reactions is given below.

(R20) $H_2O_2(+M)=OH+OH(+M)$

The dissociation of H_2O_2 radicals is characterized by many researchers as the central kinetic feature in the operation of HCCI engines, or the key factor for the abnormal combustion phenomena, such as engine knock, in SI engines [49, 50]. This is because the decomposition of H_2O_2 via R20 gives access for secondary reactions and forms very reactive OH radicals [51]. Two different studies have been conducted to investigate the low-pressure limit and high-pressure limit rate constants. First Hong et al. [52], investigated R20 by using a laser absorption diagnostics for H_2O and OH [52, 53] at 1.8 atm pressure. Their results were in agreement with a previous study by Kappel et al. [51], although they have lower experimental uncertainty. They suggested a new lower-pressure limit rate constant for R20 and a high-pressure limit rate constant from a different study conducted by Sellevag [54]. The second study, conducted by Troe et al [55], suggests new pressure dependent rate constants by performing a theoretical study based on experimental data. Due to the lower level of experimental uncertainty Hong's set of rate constants has been adopted in this study for R20.

Other studies showed that at higher pressures, H_2O_2 concentration increases during $H_2O_2(+M) = OH + OH(+M)$ reaction [56]. This is because at higher pressures, the high concentration of the mixture, including enhanced third-body efficiencies M, leads to a sufficient concentration of HO_2, which is less reactive than other free radicals, forming H_2O_2. Before high temperatures are reached, the characteristic reaction time of H_2/CO mixtures is long [34]. This reduction in reaction sensitivity causes the H_2O_2 concentration to increase. It was also shown that as the equivalence ratio increases, the H_2O_2/OH ratio gradually decreases and the higher syngas initial H_2 concentration provides an enhanced chain-initiation process through $H_2 + O_2 \rightarrow OH + OH$ or $H_2 + O_2 \rightarrow H + HO_2$ reactions, ensuring the occurrence of subsequent chain-branching reactions along with an increase in the OH concentration.

(R24) $H+O_2(+M)=>HO_2(+M)$

R24 has a key role in hydrogen combustion and is responsible for the reactivity at low temperatures [35]. Therefore, the temperature and pressure dependence of the chain propagation reaction R24 has been studied extensively by many researchers [42]. Fernandes et al [57], proposed pressure and temperature dependent rate constant for a temperature range between 300 -900 K and a pressure range between 1.5 to 900 bars. The authors have tried to extend the temperature and pressure range by using the unimolecular rate theory. However, at temperature ranges from 1000 to 1200 K, the mixture reactivity decreased significantly while the ignition delay time increased. This is because of the low pressure limit rate constant which uses argon as a bath gas. Bates et al. [58] studied the pressure and temperature dependence of R24 at temperature ranges from 1020 to 1260 K and pressure ranges from 10 to 50 bars by using argon. They proposed low pressure limit rate constant that was in a good agreement with the experimental data.

Finally, during a new study by Keromnes et al. [35], a “hybrid’’ expression of rate constant was used by combining the high pressure limit rate constants proposed by Fernandes [57] and the low pressure limit rate constant proposed by Bates et al. [58]. The new hybrid rate constants showed a good agreement with the

365 experimental data at all the temperature and pressure ranges. Therefore, in our mechanism we adopted the new
366 rate constants proposed by Keromnes et al. [35].
367
368 *(R21) $H+O_2=OH+O$*
369 R21 is one of the most important reactions in the syngas chemical reaction mechanism. It is a leading reaction
370 which is responsible for the control of the fuels oxidation at temperatures higher than 1000 K [35]. Because of
371 its sensitivity, the rate constants used in different mechanisms vary. For example, the rate constant proposed by
372 Piraglia et al. [59] were adopted by Muller et al. [60] and Oconnair et al. [61], in order to reproduce more
373 accurate explosion limit at temperatures between 680-900 K. Other authors such as Keromnes et al. [35] used a
374 rate constant proposed by Hong et al. [62], which has 10% uncertainty at temperature ranges from 1100 to
375 3370 K. During this study the rate constant from Fernandes Gallisteo et al. [63] was adopted to show a good
376 agreement with the experimental results.
377
378
379 *(R31) $H_2O_2+H=H_2+HO_2$*
380 This reaction is very important under low temperatures and high pressure conditions. The consumption of one
381 HO_2 radical leads to the production of one H_2O_2 molecule. The decomposition of H_2O_2 will, in turn, lead to the
382 formation of two high reactive OH radicals [35]. Therefore it can be said that R31 is responsible for the
383 increase of the reactivity. Due to its high sensitivity this reaction has been studied in detail by many authors in
384 order to find the best rate constants [42]. The rate constants recommended by Tsang et al. [64] is by a factor of
385 3 higher than the rate constants recommended by Baulch et al. [65]. Different rate constants result in different
386 ignition delay times, as shown by Keromnes et al. [35]. For example at 50 bar and 1000K the ignition delay
387 times obtained by Baulch et al. [65] were by a factor of 3 different than the ignition delay times obtained by
388 Tsang et al. [64]. During a study by Ellingson et al. [66] the rate constants are calculated by using the canonical
389 variational transition state theory. The calculated ignition delay times from Ellingson approach were in a good
390 agreement with Mittal et al. calculations [67]. The rate constant recommended by Konnov [42] was adopted

with exponential factor A = 7.7E12, which lies within the stated level of uncertainty, in order to get the best agreement of our mechanism with the experimental data and with the ignition delay times from other already proposed mechanisms.

(R9) $CO+OH=CO_2+H$

According to Li et al. [40], the laminar flame speed and the mixture reactivity are sensitive to R9 [68]. Therefore, in order to obtain the best agreement with the experimental data and the laminar flame speed measurements the reaction constants proposed by Frassoldati et al. [25] were used in this study.

(R4) $CH_4+OH=CH_3+H_2O$

This reaction is responsible for the consumption of CH_4 and the formation of CH_3 radicals. Different rate constants have been proposed in the literature and used in different chemical reaction mechanisms by different researchers. The rate constant used for GRI Mech 3.0 [32] was based on the Cohen's Transition State Theory and validated against experimental data [69]. Baulch et al. [70] also proposed a new rate constant based on the study of Madronich and Felder [71] with an extended temperature range from 250 to 2500 K. Srinivasan et al. [72] on the other hand proposed a new non-Arrhenius expression for a temperature range between 195-2025 K. Li and Williams [73] used a rate constant for R4 which shows a good level of accuracy and it was in a good agreement with the measured and calculated data. In our study we used the rate constant from Li and Williams [73] which gave a good match with our experimental results.

(R5) $CH_3+O_2=CH_2O+OH$

One of the most important reactions for the accurate prediction of methane ignition delay time is R5 [74]. The importance of that reaction forced researchers to investigate in detail the temperature and pressure dependence of R5 and propose different rate constants. For example, the rate constant used in San Diego mechanism [75] is higher by a factor of forty-two from the rate constant used in GRI Mech 3.0 [32]. The rate constant proposed by Srinivasan et al. [76], is one order of magnitude lower than the rate constant suggested by Herbon et al. [77].

In our mechanism we used the rate constants proposed by Frassoldati et al. [25].

(R22) H_2+O=OH+H

The consumption and the production of hydrogen radicals play a key role on the ignition delay times and the laminar flame speed and in general are very important for the in-cylinder combustion. Therefore, reactions which are responsible for the production of H radicals have been investigated in deep by different researchers in order to find the most accurate rate constant during low and high temperature and pressure conditions. R22 is responsible for the production of H and OH radicals. The production of OH radicals leads to the initiation of reaction R23 which will be discussed in the next paragraph. According to a review by Baulch et al. [78], the most accurate rate constant for R22 was proposed by Sutherland et al. [79]. The expression from Sutherland is compared with the measurements from Natarajan and Roth [80] at temperature range from 1713 to 3532 K, with Davidson and Handson [81] validated at ranges from 2120-2750 K and finally tested by Javoy et al. [82] at temperatures 2690-3360 K. For all of the temperature ranges the expression proposed by Sutherland showed a very good agreement with the measurements. During this study we used the rate constant which were proposed by Sutherland [79].

(R23) H_2+OH=H_2O+H

The production of OH radicals from R22, triggers R23. The reaction between H_2 and OH radicals leads to the conversion of OH to H atoms. Laminar flame speed and ignition delay times are also very sensitive to this reaction [83]. Many researchers investigated the rate constants and proposed a value to accurately predict the sensitivity of this reaction to the temperature changes. For temperature ranges between 300 and 2500 K, Baulch et al. [78] proposed a new rate constant which was used also by Konnov [84, 85]. However, a second research by Baulch et al. [65] based on the work of Michael et al. [86] and Oldenborg et al. [87], showed that R23 is very sensitive to the temperature changes. At 300 K the uncertainty factor of R23 was 1.2 increasing to 2 at temperature 2500 K [65]. Therefore, a new rate constant has been proposed by Baulch et al. [65] in order

to satisfy the uncertainty of R23 at different temperatures. In this study we used the rate constant proposed by Sutherland et al. [79].

(R18) $O_2+CO=CO_2+O$

According to a research by Saxena et al. [20], although reaction 18 does not affect the laminar burning velocities, it is very important for the ignition initiation and the ignition delay times especially at lower hydrogen content. This reaction is therefore an essential reaction and is added to the mechanisms by using the rate constant from Frassoldati et al [25].

(R2) $CH_4 + O_2 = CH_3 + HO_2$

The preignition chemistry of methane is initiated primarily by this reaction. At high pressures or in the initial stages of hydrocarbon oxidation, high concentrations of HO_2 can initiate reaction $CO + HO_2 = CO_2 + OH$ [88]. Thus, CO oxidation at high pressures can be modelled by adding reaction $CO + HO_2 = CO_2 + OH$ to the syngas kinetics mechanism, as shown by Kim *at al*. [89]. This reaction is the most sensitive of the CO subsystems under the conditions investigated. The rate constant used for this reaction was updated taking the rate constant from Li and Williams [46] that was originally proposed by Lindstedt and Skevis [90].

(R29) $OH+HO_2=H_2O+O_2$

A recent study by Keromnes et al. [35] showed that R29 is very sensitive to the fuel-lean flames. Many theoretical and experimental studies have been conducted in order to analyse the dependency of the reaction rate constants on the temperature [66, 91-92]. However, at temperatures around 1250 K, unusual temperature dependence is observed which leads to a non-Arrhenius behaviour and creates a deep minimum for the calculated rate constant [35]. This makes the reproduction of the temperature dependence very difficult and creates high level of uncertainties [42]. Recent investigations by Hong et al. [93] and Burke et al. [92], showed that R29 has a weak temperature dependence but they also concluded that future work is required to ensure the accuracy of the rate constants at temperatures between 900-1200 K. In this study we used rate constants defined by Keromnes et al. [35].

3.2 Ignition delay

Ignition delay time simulations were performed using RCM model in DARS. Ignition delay time obtained using the new mechanism was compared with that obtained by Keromnes et al. [35], Frassoldati et al. [25] and GRI Mech 3.0 [32] for four types of syngas compositions at T=800-1053K, P=225kPa and ϕ=0.63. Figure 2 shows that the ignition delay time for the new mechanism matches very well with those obtained using different tested mechanisms in the broad range of temperatures for all syngas types investigated in this paper. Figures 3 and 4 show the ignition delay times for new mechanism at high pressures. Analysis was performed for syngas type 1 at temperature range 800-1053K and ϕ=0.63, and syngas type 2 at temperature range 800-1053K and ϕ=0.83. The results obtained by using new mechanism were in a good agreement with the ignition delay times obtained by using Frassoldati et al. [25] and Keromnes et al. [35] mechanisms and in exceptionally good agreement with ignition delay times obtained by using GRI Mech 3.0 [32] mechanism.

We also compared the ignition delay times using syngas mixture compositions defined in Table 4 from the University of Connecticut. The study has been performed under stoichiometric conditions with 50%, 25% and 10% H_2 in the H_2/CO fuel mixtures at the end-of-compression temperature range of 914-1068K using the new mechanism and mechanism reported by Keromnes et al. [35]. Results on Figure 5 show the inhibiting effect of carbon monoxide on the syngas ignition delay times, which increase with increasing amounts of CO in the syngas mixture. The new mechanism captures this inhibiting effect accurately and its predictions are in a very good agreement.

3.3 Flame speed

The flame speed analysis was performed to compare the laminar flame speed obtained using the new mechanism with that of Keromnes et al. [35], Frassoldati et al. [25] and GRI Mech 3.0 [32]. Figure 6 shows that for syngas types 1-4 over a range of equivalence ratios, the new mechanism showed the identical trend in

laminar flame speed as the one obtained using above mentioned mechanisms. For syngas type 4, GRI Mech 3.0 mechanism slightly over predicted the laminar flame speed. This is due to the high H_2 concentration in the type 4 syngas. GRI Mech 3.0 was developed to simulate mainly natural gas combustion and was not designed to predict the oxidation of fuel with high H_2 content. Figure also shows that laminar flame speed for syngas type 2 is slightly higher due to higher H_2 concentration compared to syngas types 1 and 3.

Using new mechanism we evaluated laminar flame speed for $H_2/CO/CO_2$ mixtures and compared the results with experimental data by Hu et al. [94] and predictions from the different kinetics models [25, 32, 35] over a range of equivalence ratios, ϕ=0.4-1.0. Figure 7 shows the flame speed calculated using the chemical kinetics mechanisms for $H_2/CO/CO_2$ – 35:35:30 mixture at different pressures and temperatures. The new mechanism performed remarkably well at predicting the laminar flame speed across all the equivalence ratios investigated by Hu et al. [94].

In this study, we also considered the laminar flame speed of H_2/CH_4 at a range of CH_4 ratios and equivalence ratios to evaluate the new mechanism. Figure 8 shows the laminar flame speed for various H_2:CH_4 ratios at T=298K and P=1atm and equivalence ratio ranging from 0.4 to 1.2. For H_2/CH_4 mixtures the laminar flame speed results obtained with the new mechanism exhibit the best agreement with the laminar speed data obtained using Keromnes et al. [35] and GRI Mech 3.0 [32] mechanisms.

Laminar flame speed was also evaluated at high pressures. Figure 9 shows that at P=20 bar the laminar speed data obtained using the new mechanism matches well with those obtained using GRI Mech 3.0 mechanism, showing slight deviation from the laminar flame speed obtained using Keromnes et al. [35] and Frassoldati et al. [25] mechanisms. However, this difference gradually disappears at lower equivalence ratio levels, those usually used in dual-fuel engine combustion. At high pressure of 80 bar the laminar flame speed data matches well for all tested mechanisms and equivalence ratios.

4. Results and Discussion

4.1 Mechanism validation for CFD combustion analysis

To validate the mechanism for the engine in-cylinder-like conditions in a dual-fuel engine, an analysis was performed by applying a pilot injection using the coupled CFD and syngas chemical kinetics mechanism. Figure 10 compares the in-cylinder pressure obtained by a new mechanism using CFD code with that of Slavinskaya et al. [27], Keromnes et al. [35], Frassoldatti et al. [25], GRI Mech 3.0 [32] and engine experiment. Figure 10 shows that new mechanism accurately simulates the engine in-cylinder combustion for syngas with different compositions where other syngas mechanisms show very large deviation from experiments. A similar trend was observed for a range of different equivalence ratios and injection timings.

4.2 Chemical kinetics mechanism for syngas with high H2 content

The developed mechanism showed good match between simulation results and experimental data for syngas Types 1-3 (biomass solid feedstock) at various equivalence ratios and injection timings. However, with this mechanism the combustion rate was much higher for syngas Type 4 (coke-oven solid feedstock). The higher combustion rate was due to the effect of higher H_2, higher CH_4 and lower CO gas concentrations.

The rate constants for reaction $H_2O_2+H=H_2+HO_2$ were replaced by constants from different mechanisms as it was expected that with higher H_2 concentration the in-cylinder combustion rate would be affected by this reaction. This reaction is very important under low temperature and high pressure conditions. The consumption of one HO_2 radical leads to the production of one H_2O_2 molecule. The decomposition of H_2O_2 will, in turn, lead to the formation of two high reactive OH radicals via H_2O_2 (+M)=OH+OH (+M) [35]. Due to its high sensitivity $H_2O_2+H=H_2+HO_2$ reaction has been studied in detail by many authors in order to find the best-matching rate constants [42]. In fact, we can find a great variety in rate constant values used for different syngas chemical kinetic mechanisms. Konnov [42] proposed a new rate constant for reaction $H_2O_2+H=H_2+HO_2$ which is based on a new research by Baulch et al. [65]. Konnov [42] reevaluated $H_2O_2+H=H_2+HO_2$ rate constants and increased the uncertainty factor to 3.

We performed the reaction sensitivity study using the modified mechanism for syngas with a higher H_2

548 content. It shows the high sensitivity of $H_2O_2(+M)=OH+OH(+M)$, $H_2O_2+H=H_2+HO_2$, and
549 $HO_2+HO_2=H_2O_2+O_2$ reactions and low sensitivity of $HO_2+H=OH+OH$ reaction. It should be noticed that
550 reactions R7, R27 and R30 were not shown as sensitive in Figure 1 when the original mechanism was applied
551 to syngas type 1 (H_2-13.7%), and showed strong sensitivity in Figure 11 when modified mechanism was
552 applied to syngas type 4 (H_2-56.8%). Brief description of these three reactions is given below:
553
554 *(R7) $CO+O(+M)=CO_2(+M)$*
555 R7 is responsible for the conversions of CO to CO_2 and is very sensitive at high pressures and high
556 temperatures. In order to estimate accurately the dependence of R7 on the temperature and pressure, low
557 pressure limit rate constants must be used [95]. For this research we used the high and low pressure limit rate
558 constants which were proposed by Frassoldati et al. [25] and validated against experimental data.
559
560 *(R27) $HO_2+H=OH+OH$*
561 According to O'Conaire et al. [96], changing the rate constant of R27 has an adverse effect on the results of the
562 flow reactor simulations. They suggested a rate constant for R27 which is within the limits of the experimental
563 data obtained from the NIST database [97], and has lower uncertainty factor. In this paper the rate constants
564 proposed by O'Conaire [96] were adopted because they are within the limits of the experimental data.
565
566 *(R30) $HO_2+HO_2=H_2O_2+O_2$*
567 This reaction is very sensitive during low temperature and high pressure conditions [98]. Both reactions, R30
568 with R31, contribute to the formation of H_2O_2 which in turn decomposes into two highly reactive OH radicals
569 through reaction R20. However, it can be said that R30 and R31 are competitors; in which R30 increases the
570 reactivity as it produces two HO_2 radicals while R31 inhibits the reactivity as it produces only one HO_2 radical.
571 The set of rate constants used by Keromnes et al. [35] was chosen for this study.
572 Comparison of two sensitivity analysis for Type 1 shown in Figure 1 and Type 4 shown in Figure 11
573 suggests that for Type 1, with lower H_2 content, more carbon-based reactions play important role in chemical
574 kinetics, whereas, for Type 4 with higher H_2 content the number of hydrogen-based sensitive reactions

prevailed. Figures 12 and 13 show the flow of species of carbon and hydrogen in syngas Type 1 and Type 4. It is seen that for carbon atoms of both syngas types, the major paths represent the high-temperature hydrocarbon oxidation of CH_4 through CH_3 and further oxidation of CH_3 to CH_2O.

Fluxes for H below 1% of maximum flow have been filtered. The flow analysis for hydrogen species at lower H_2 content of syngas (Type 1, Type 2 and Type 3) showed the identical flow pattern at pressures 10, 30 and 50 bar as shown in Figure 13. However, when hydrogen concentration in the syngas increases more than 50 % (Type 4) flow from H_2O_2 to OH and back increases as the pressure increases. It was observed that at high pressures the effect of H atom becomes noticeable to contribute to HO_2 formation.

Ignition delay time and laminar flame speed obtained using modified mechanism were compared with those obtained using Keromnes et al. [35], Frassoldati et al. [25] and GRI Mech 3.0 [32] and the new mechanism. Figure 14 shows that modified mechanism that is tend to simulate syngas with high H_2 concentration accurately predicted ignition delay and laminar flame speed. To estimate the effect of different rate constants on the in-cylinder heat production and pressure rise, the mechanism was tested by running 3D CFD analysis with reaction rate constants proposed by different authors. Figure 15 shows in-cylinder pressure CFD results for syngas composition of Type 4. $H_2O_2+H=H_2+HO_2$ reaction constants proposed by Hong et al. [49] and adjusted power factor n = 0.0 showed the closest match with experimental data.

4.3 In-cylinder 3D combustion analysis

To validate the new mechanism shown in Table 3 for the in-cylinder-like conditions in a dual-fuel engine, an analysis was performed by applying a micro-pilot injection using the coupled CFD and developed syngas chemical kinetics mechanism. The pressure and ROHR plots shown in Figure 16 show a good match between the simulation results and experimental data for different types of syngas at various equivalence ratios and injection timings. Conditions A-B, C-D and E-F were simulated using the new chemical kinetics mechanism, and conditions G-H were simulated using the modified mechanism with constants for reaction R31 adopted

599 from Hong et al. [49] with adjusted power factor n = 0.0. Figure 17 shows the crank angle resolved in-cylinder
600 spray and temperature distribution for syngas type 1 and type 4. The images show micro-pilot injected
601 n-heptane spray development with further ignition and combustion of syngas. The maximum in-cylinder
602 spatial temperature reached about 2200K and it is seen that the flame front propagates towards the cylinder
603 wall gradually consuming the unburned in-cylinder mixture and the fuel is fully burned. The files with
604 animation of the full combustion process for these two conditions are attached to this manuscript as
605 supplementary material.
606
607 **5. Conclusion**
608 This study presents a new CFD-compatible syngas chemical kinetics mechanism based on the flow and
609 reaction sensitivity analysis and CFD simulations. The developed syngas mechanism was validated in a
610 supercharged dual-fuel engine with various syngas initial compositions under lean conditions concurrently by
611 using a chemical kinetics code and a multidimensional CFD code. The results were compared with
612 experimental data of combustion and syngas chemical kinetics mechanisms developed by other researchers.
613 Ignition delay time and laminar flame speed results predicted by using the new mechanism are in a very good
614 agreement with those obtained by using other validated syngas mechanisms. Sensitivity analysis showed that
615 the reactivity of syngas mixtures was found to be governed by hydrogen and CO chemistry for H_2
616 concentrations lower than 50% and mostly by hydrogen chemistry for H_2 concentrations higher than 50%. In
617 the mechanism validation, particular emphasis is placed on predicting the combustion under high pressure
618 conditions. For high H_2 concentration in syngas under high pressure, the reactions $HO_2+HO_2=H_2O_2+O_2$ and
619 $H_2O_2+H=H_2+HO_2$ were found to play important role affecting the in-cylinder combustion rate and heat
620 production. The rate constants for $H_2O_2+H=H_2+HO_2$ reaction showed strong sensitivity to high-pressure
621 ignition times and has considerable uncertainty. To accurately simulate syngas derived from coke-oven
622 feedstock with high H_2 concentration some modifications to a new mechanism were introduced. In particular,

constants for reaction R31 were adopted from Hong et al. [49] with adjusted power factor n = 0.0. and reactions $HO_2+OH=H_2O+O_2$ and $O+H_2O=OH+OH$ were excluded from the mechanism. These reactions did not appear in the list of the most sensitive reactions. In fact, they are not contributing to the further chain branching and chain propagation where H radical presence is required.

Developed mechanism was used in CFD analysis to predict in-cylinder combustion of syngas and results were compared with experimental data. The new mechanism predicted the in-cylinder combustion performance well for both biomass and coke-oven syngas in a micro-pilot ignited supercharged dual-fuel engine, including the cylinder pressure history and heat-release rate data with respect to syngas composition, equivalence ratio, and injection timing.

Acknowledgements

The authors are grateful to the Faculty of Engineering and Environment of Northumbria University for providing funding for this work through RDF studentship.

The English in this document has been checked by at least two professional editors, both native speakers of English.

References

[1] Sridar G, Paul PJ, Mukunda HS. Biomass derived producer gas as a reciprocating engine fuel-an experimental analysis. Biomass and Bioenergy 2001;21:61-72.

[2] Shilling NZ, Lee DT. IGCC-Clean power generation alternative for solid fuels: GE Power Systems. PowerGenAsia 2003.

[3] Shudo T, takahashi T, Influence of reformed gas composition on HCCI combustion engine system fueled with DME and H_2-CO-CO_2 which are onboard-reformed from methanol utilizing engine exhaust heat. Trans.JSME B 2004;70:2663.

[4] Shudo T. An HCCI combustion engine system using on-board reformed gases of methanol with waste heat recovery: Ignition control by hydrogen. Int J Veh Design 2006;41:206.

[5] Li H, Karim GA. Exhaust emissions from an SI engine operating on gaseous fuel mixtures containing hydrogen. Inj J Hydrogen Energy 2005;30:1491.

[6] Karim G.A. Combustion in gas fueled compression: Ignition engines of the dual fuel type. J. Eng. Gas Turb.

655 Power 2003;125:827-836.

656 [7] Liu Z, Karim GA. Simulation of combustion process in gas-fuelled diesel engine. Proc Inst Mech Eng
657 A:11.

658 [8] Poonia MP, Ramesh A, Gaur RR. Effect of intake air temperature and pilot fuel quantity on the combustion
659 characteristics of a LPG-diesel dual-fuel engine. SAE Paper, 982455.

660 [9] Karim GA, Moore NPW. The production of hydrogen by the partial oxidation of methane in a dual-fuel
661 engine. SAE Paper, 901501.

662 [10] Karim GA, Wierzba I. Safety measures associated with the operation of engines on various alternative
663 fuels. Reliability Eng Syst Safety 1992;37:93.

664 [11] McMillian MH, Lawson SA. Experimental and modeling study of hydrogen/syngas production and
665 particulate emissions from a natural gas-fuelled partial oxidation engine. Int J Hydrogen Energy 2006;31:847.

666 [12] Christodoulou F, Megaritis A. The effect of reformer gas mixture on the performance and emissions of an
667 HSDI diesel engine. Int J Hydrogen Energy 2014;39:9798.

668 [13] Bilcan A. Contribution to the study of the thermodynamic cycle of dual-fuel. PhD Thesis 2003, Nantes
669 University, France.

670 [14] Baratieri M, Baggio P, Bosio P, Grigiante M, Longo GA. The use of biomass syngas in IC engines and
671 CCGT plants: A comprehensive analysis. Applied Therm Engineering 2009;29:3309-3318.

672 [15] Boehman AL, Le Corre O. Combustion of syngas in internal combustion engines. Combust Sci Tech
673 2008;180:1193-1206.

674 [16] Tomita E, Fukatani N, Kawahara N, Maruyama K, Komoda T. Combustion characteristics and
675 performance of supercharged pyrolysis gas engine with micro-pilot ignition. CIMAC congress 2007. Paper No.
676 178.

677 [17] Roy MM, Tomita E, Kawahara N, Harada Y, Sakane A. Performance and emission comparison of a
678 supercharged dual-fuel engine fueled by producer gases with varying hydrogen content. Int J Hydrogen Energy
679 2009;34:7811-22.

680 [18] Roy MM, Tomita E, Kawahara N, Harada Y, Sakane A. Performance and emissions of a supercharged
681 dual-fuel engine fueled by hydrogen-rich coke oven gas. Int J Hydrogen Energy 2009;34:9628-38.

682 [19] Yetter RA, Dryer FL, Rabitz H. A comprehensive reaction mechanism for carbon
683 monoxide/hydrogen/oxygen kinetics. Combust Sci Tech 1991;79:97.

684 [20] Saxena P, Williams FA. Testing a small detailed chemical-kinetic mechanism for the combustion of
685 hydrogen and carbon monoxide. Combust Flame 2006;145:316-323.

686 [21] Dowdy DR, Smith DB, Taylor SC, Williams A. The use of expanding spherical flames to determine
687 burning velocities and stretch effects in hydrogen-air mixtures. Proc Combust Inst 1990; 23:325.

688 [22] Egolfopoulos FN, Law CK. An experimental and computational study of the burning rates of ultra-lean to
689 moderately rich $H_2/O_2/N_2$ laminar flames with pressure variations. Proc Combust Inst 1990;23:333.

690 [23] Tse SD, Zhu DL, Law CK. Morphology and burning rates of expanding spherical flames in H2/O2/inert
691 mixtures up to 60 atmospheres. Proc Combust Inst 2000;28:1793.

692 [24] Kwon OC, Faeth GM. Flame/stretch interactions of premixed hydrogen-fueled flames: measurements and

predictions. Combust Flame 2001;124:590.

[25] Frassoldati A, Faravelli T, Ranzi E. The ignition, combustion and flame structure of carbon monoxide/hydrogen mixtures. Note 1: Detailed kinetic modeling of syngas combustion also in presence of nitrogen compounds. Int J Hydrogen Energy 2007;32:3471-3485.

[26] Cuoci A, Frassoldati A, Buzzi Ferraris G, Faravelli T, Ranzi E. The ignition, combustion and flame structure of carbon monoxide/hydrogen mixtures. Note 2: Fluid dynamics and kinetic aspects of syngas combustion. Int J Hydrogen Energy 2007;32:3486-3500.

[27] Slavinskaya N, Braun-Unkhoff M, Frank P. Reduced reaction mechanisms for methane and syngas combustion in gas turbines. J Engr Gas Turb Power 2008;130:(021504)1-6.

[28] Starik AM, Titova NS, Sharipov AS, Kozlov VE. Syngas oxidation mechanism. Combust Expl Shock Waves 2010;46:491-506.

[29] Sun H, Yang SI, Jomaas G, Law CK. High-pressure laminar flame speeds and kinetic modeling of carbon monoxide/hydrogen combustion. Proc Combust Inst 2007;31:439-446.

[30] Sivaramakrishnan R, Comandini A, Tranter RS, Brezinsky K, Davis SG, Wang H. Combustion of CO/H_2 mixtures at elevated pressures. Proc Combust Inst 2007;31:429-437.

[31] Cavaliere DE, De Ioannon M, Sabia P, Allegorico M, Marchione T, Sirignano M, D'Anna A. A comprehensive kinetic modeling of ignition of syngas/air mixtures at low temperatures and high pressures. Combustion Colloquia 2009, 32nd Meeting on Combustion of the Italian Section of the Combustion Institute, April 26-28, Napoli, University Federico II, 26-28 of April, 2009.

[32] Smith GP, Golden DM, Frenklach M, Moriarty NW, Eiteneer B, Goldenberg M, Bowman CT, Hanson RK, Song S, Gardiner WC, Jr., Lissianski VV, and Qin Z GRI-Mech home page http://www.me.berkeley.edu/gri_mech/

[33] Mittal G, Sung CJ, Fairweather M, Tomlin AS, Griffiths JF, Hughes KJ. Significance of the HO_2+CO reaction during the combustion of CO+H_2 mixtures at high pressures. Proc Combust Inst 2007;31:419-427.

[34] Chaos M, Fryer FL. Syngas combustion kinetics and applications. Combust Sci Tech 2008;180:1053-1096.

[35] Kéromnès A, Metcalfe WK, Heufer KA, Donohoe N, Das AK, Sung CJ, Herzler J, Naumann C, Griebel P, Mathieu O, Krejci M, Petersen EL, Pitz WJ, Curran HJ. An experimental and detailed chemical kinetics modeling study of hydrogen and syngas mixture oxidation at elevated pressures. Combust Flame 2013;160:995-1011.

[36] Lee HC, Mohamad AA, Jiang LY. Comprehensive comparison of chemical kinetics mechanisms for syngas/biogas mixtures. Energy Fuels 2015;29:6126-6145.

[37] Metcalfe WK, Burke SM, Ahmed SS, Curran HJ. A Hierarchical and Comparative Kinetic Modeling Study of $C_1 - C_2$ Hydrocarbon and Oxygenated Fuels. Int J Chem Kinet 2013;45:638-675.

[38] Olm C, Zsely IG, varga T, Curran HJ, Turanyi. Comparison of the performance of several recent syngas combustion mechanisms. Combust Flame 2015;162:1793-1812.

[39] Healy D, Kalitan DM, Aul CJ, Petersen EL, Bourque G, Curran HJ. Oxidation of C_1-C_5 Alkane Quinternary Natural Gas Mixtures at High Pressures. Energy Fuels 2010;24:1521-1528.

[40] Li J, Zhao Z, Kazakov A, Chaos M, Dryer FL, Scire JJJ. A comprehensive kinetic mechanism for CO,

CH_2O, and CH_3OH combustion. Int J Chem Kinet 2007;39:109-136.

[41] Kong SC, Reitz RD. Use of detailed chemical kinetics to study HCCI engine combustion with consideration of turbulent mixing effects. J Eng Gas Turb Power 2002;124:702-707.

[42] Konnov A. Remaining uncertainties in the kinetic mechanism of hydrogen combustion. Combust Flame 2008;152:507-528.

[43] 2015 CD-Adapco Inc., DARS Basic 2.10.

[44] Reitz RD, Diwakar R. Effect of drop breakup on fuel sprays. SAE paper, 860469.

[45] Reitz RD, Diwakar R. Structure of high-pressure fuel spray. SAE paper, 870598.

[46] Li SC, Williams FA. A reduced reaction mechanism for predicting knock in dual-fuel engines. SAE Paper 2000-01-0957.

[47] 2015 CD-Adapco Inc. Methodology, Star-CD V4.2

[48] Donkerbroek AJ, van Vliet AP, Somers LMT, Frijters PJM, Klein-Douwel RJH, Dam NJ, Meerts WL, ter Meulen JJ. Time- and space-resolved quantitative LIF measurements of formaldehyde in a heavy-duty diesel engine. Combust Flame 2010;157:155-166.

[49] Hong Z, Davidson DF, Hanson RK. An improved H2/O2 mechanism based on recent shock tube/laser absorption measurements. Combust Flame 2011;158:633-644.

[50] Westbrook CK. Chemical kinetics of hydrocarbon ignition in practical combustion systems. Proc. Combust. Inst 2000;28:1563–1577.

[51] Kappel C, Luther K, Troe J. Shock wave study of the unimolecular dissociation of H2O2 in its falloff range and of its secondary reactions. Phys Chem Chem Phys 2002;4:4392–4398.

[52] Hong Z, Farooq A, Barbour EA, Davidson DF, Hanson RK. Hydrogen peroxide decomposition rate: A shock tube study using tunable laser absorption of H2O near 2.5 μm. J Phys Chem 2009;113:12919–12925.

[53] Hong Z, Cook RD, Davidson DF, Hanson RK. A shock tube study of OH + H_2O_2 —> H_2O + HO_2 and H_2O_2 + M —> 2OH + M using laser absorption of H_2O and OH. J Phys Chem 2010;114:5718–5727.

[54] Sellevag SR, Georgievskii Y, Miller JA. Kinetics of the gas phase recombination reaction of hydroxyl radicals to form hydrogen peroxide. J Phys Chem 2009;113:4457–4467.

[55] Troe J. The thermal dissociation/recombination reaction of hydrogen peroxide H2O2(+M) ↔ 2OH(+M) III. Analysis and representation of the temperature and pressure dependence over wide ranges. Combust. Flame 2011;158:594–601.

[56] Azimov U, Okuno M, Tsuboi K, Kawahara N, Tomita E. Multidimensional CFD simulation of syngas combustion in a micro-pilot-ignited dual-fuel engine using a constructed chemical kinetics mechanism. Int J Hydrogen Energy 2011:36:13793-13807.

[57] Fernandes RX, Luther K, Troe J, Ushakov VG. Experimental and modelling study of the recombination reaction H + O2(+M) → HO2 (+M) between 300 and 900 K, 1.5 and 950 bar, and in the bath gases M = He, Ar, and N2. Phys Chem Chem Phys 2008;10:4313–4321.

[58] Bates RW, Golden DM, Hanson RK, Bowman CT. Experimental study and modeling of the reaction H + O2+ M → HO2+ M (M = Ar, N2, H2O) at elevated pressures and temperatures between 1050 and 1250 K. Phys Chem Chem Phys 2001;3:2337–2342.

[59] Pirraglia AN, Michael JV, Sutherland JW, Klemm RB. A flash photolysis-shock tube kinetic study of the H-atom reaction with O2: H + O2 → OH + O (962 ≤ T ≤ 1705 K) and H + O2 + Ar → HO2 + Ar (746 < T < 987 K). J Phys Chem 1989;93:282–291.

[60] Mueller MA, Kim TJ, Yetter RA, Dryer FL. Flow reactor studies and kinetic modeling of the H2/O2 reaction. Int J Chem Kinet 1999;31:113–125.

[61] O'Conaire M, Curran HJ, Simmie JM, Pitz WJ, Westbrook CK. A comprehensive modeling study of hydrogen oxidation. Int J Chem Kinet 2004;36:603–622.

[62] Hong Z, Davidson DF, Barbour EA, Hanson RK. A new shock tube study of the H + O2 → OH + O reaction rate using tunable diode laser absorption of H2O near 2.5 μm. Proc. Combust Inst 2011;33:309–316.

[63] Fernandez-Galisteo D, del Alamo G, Sanchez AL, Linan A. Zeldovich analysis of hydrogen-air premixed flames. In: Proceedings of the Europian Combustion Meeting 2007.

[64] Tsang W, Hampson RF. Chemical kinetic database for combustion chemistry. Part I. Methane and related compounds. J. Phys. Chem. Ref. Data 1986;15:1087–1280.

[65] Baulch DL, Bowman CT, Cobos CJ, Cox RA, Just T, Kerr JA, Pilling MJ, Stocker D, Troe J, Tsang W, Walker RW, Warnatz J. Evaluated kinetic data for combustion modeling: Supplement II. J. Phys. Chem. Ref. Data 2005;34:757–1397.

[66] Ellingson BA, Theis DP, Tishchenko O, Zheng J, Truhlar DG. Reactions of hydrogen atom with hydrogen peroxide. J. Phys. Chem. A 2007;111:13554–13566.

[67] Mittal G, Sung CJ, Yetter RA. Autoignition of H2/CO at elevated pressures in a rapid compression machine. Int J Chem Kinet 2006;38:516-529.

[68] Zhao ZW, Li J, Kazakov A, Dryer FL. Temperature-dependent feature sensitivity analysis for combustion modelling. Int. J. Chem. Kinet. 2005;37:282–295.

[69] Cohen N. Are reaction rate coefficients additive? Revised transition state theory calculations for OH + alkane reactions. Int J Chem. Kinet 1991;23:397-417.

[70] Baulch DL, Cobos CJ, Cox RA, Frank P, Hayman G, Just Th, Kerr JA, Murrells T, Pilling MJ, Troe J, Walker RW, Warnatz J. Evaluated kinetic data for combustion modeling. Supplement I. J Phys Chem Ref Data 1994;23:847.

[71] Madronich S, Felder W. Direct measurements of the rate coefficient for the reaction OH+CH4 → CH3+H2O over 300-1500 K. Proc Comb Inst 1984;20:703-713.

[72] Srinivasan NK, Su MC, Sutherland W. Reflected Shock Tube Studies of High-Temperature Rate

Constants for OH+CH4→CH3+H2O and CH3+NO2→CH3O+NO. J Phys Chem A 2005;109:1857-1863.

[73] Li SC, Williams FA. Reaction mechanisms for methane ignition. J Engr Gas Turb Power 2002;124:471-480.

[74] Aul, CJ, Metcalfe WK, Burke SM, Curran HJ, Petersen EL. Ignition and kinetic modeling of methane and ethane fuel blends with oxygen: A design of experiments approach. Comb and Flame 2013;160:1153-1167.

[75] Chemical-Kinetic Mechanisms for Combustion Applications, Mechanical and Aerospace Engineering (Combustion Research), University of California at San Diego 2011.

[76] Srinivasan NK, Su MC, Sutherland JW, Michael JV. Reflected shock tube studies of high-temperature rate constants for CH3+O2, H2CO+O2, and OH+O2. J. Phys. Chem. A 2005;109:7902–7914.

[77] Herbon JT, Hanson RK, Bowman CT, Golden DM. The reaction of CH3+O2: experimental determination of the rate coefficients for the product channels at high temperatures. Proc Combust Inst 2005;30:955–963.

[78] Baulch DL, Cobos CJ, Cox RA, Frank P, Hayman G, Just T, Kerr JA, Murrells T, Pilling MJ, Troe J, Walker RW, Warnatz J. Summary table of evaluated kinetic data for combustion modeling: Supplement 1. Combust Flame 1994;98:59–79.

[79] Sutherland JW, Michael JV, Pirraglia AN, Nesbitt FL, Klemm RB. Rate constant for the reaction of $O(^3P)$ with H_2 by the flash photolysis-shock tube and flash photolysis-resonance fluorescence techniques; 504K≤T≤2495K. Proc Combust Inst 1988;21:929–941.

[80] Natarajan K, Roth P. High temperature rate coefficient for the reaction of $O(^3P)$ with H_2 obtained by the resonance absorption of O and H atoms. Combust Flame 1987;70:267–279.

[81] Davidson DF, Hanson RK. A direct comparison of shock tube photolysis and pyrolysis methods in the determination of the rate coefficient for O + H2→ OH + H. Combust Flame 1990;82:445–447.

[82] Javoy S, Naudet V, Abid S, Paillard CE. Rate constant for the reaction of O with H2 at high temperature by resonance absorption measurements of O atoms. Int J Chem Kinet 2000;32:686–695.

[83] Smith IWM, Crim FF. The chemical kinetics and dynamics of the prototypical reaction: OH + H2 → H2O + H. Phys Chem Chem Phys 2002;4:3543–3551.

[84] Konnov AA. Khim Fiz 2004;23:5–18.

[85] Konnov AA. Detailed reaction mechanism for small hydrocarbons combustion, Release 0.5, 2000.

[86] Krasnoperov LN, Michael JV. Shock tube studies using a novel multipass absorption cell: rate constant results for OH + H2 and OH + C2H6. J Phys Chem A 2004;108:5643–5648.

[87] Oldenborg RC, Loge GW, Harradine DM, Winn KR. Kinetic study of the hydrogel + hydrogen reaction from 800 to 1550 K. J Phys Chem 1992;96:8426–8430.

[88] Law CK. Combustion Physics. Cambridge University Press 2006.

[89] Kim TJ, Yetter RA, Dryer FL. New results on CO oxidation: High pressure, high temperature experiments and comprehensive kinetic modeling. Proc Combust Inst 1994;25:759-766.

[90] Lindstedt RP, Skevis G. Chemistry of acetylene flames. Combust Sci Technol 1997;125:73-137.

[91] Li J, Zhao Zh, Kazakov A, Dryer FL. An updated comprehensive kinetic model of hydrogen combustion. Int J Chem Kinet 2004;36:566-575.

[92] Burke MP, Chaos M, Ju Y, Dryer FL, Klippenstein SJ. Comprehensive H2/O2 kinetic model for high-pressure combustion. Int. J Chem Kinet 2012;44:444–474.

[93] Hong ZK, Vasu SS, Davidson DF, Hanson RK. Experimental study of the rate of OH + HO2 --> H2O + O2 at high temperatures using the reverse reaction. J Phys Chem A 2010;114:5520–5525.

[94] Hu E, Fu J, Pan L, Jiang X, Huang Z, Zhang Y. Experimental and numerical study on the effect of composition on laminar burning velocities of H2/CO/N2/CO2/air mixtures. Int J Hydrogen Energy 2012;37:18509-18519.

[95] Davis SG, Joshi AV, Wang H, Egolfopoulos F. An optimized kinetic model of H2/CO combustion. Proc Combust Inst 2005;30:1283-1292.

[96] O'Conaire M, Curran HJ, Simmie JM, Pitz WJ, Westbrook CK. A comprehensive modeling study of hydrogen oxidation. Int J Chem Kinet 2004;36:603-622.

[97] Mallard WG., Westley F, Herron JT, Hanson RF. NIST Standard Reference Database 17 2Q98; NIST Standard Reference Data: Gaithersburg, MD, 1994.

[98] Hippler H, Troe J, Willner J. Shock wave study of the reaction HO2 + HO2 = H2O2 + O2: Confirmation of a rate constant minimum near 700 K. J. Chem. Phys 1990;93:1755–1760.

FIGURE CAPTIONS

Figure 1. The 13 most sensitive reactions for syngas type 1 at 1000K and pressures 10, 30 and 50 bar.

Figure 2. Comparison of ignition delay time for syngas types 1-4 obtained with new mechanism.

Figure 3. Comparison of ignition delay time for syngas type 1 obtained with new mechanism with other mechanisms at temperatures 800-1052K, pressures 20, 40, 80 bars and equivalence ratio 0.6.

Figure 4. Comparison of ignition delay time for syngas type 4 obtained with new mechanism with other mechanisms at temperatures 800-1052K, pressures 20, 40, 80 bars and equivalence ratio 0.6.

Figure 5. Effect of CO concentration on ignition delay times of syngas mixtures compared with Keromnes et al. [35] mechanism.

Figure 6. Laminar flame speed results obtained with new mechanism for syngas types 1-4 and compared with other mechanisms.

Figure 7. Laminar flame speed of $H_2/CO/CO_2$ -35:35:30 fuel mixture at P=1-3 atm and T=303-373 K.

Figure 8. Calculated laminar flame speed of H_2/CH_4 fuel mixture obtained with new mechanism at P=1atm and T=298K and compared with different kinetic models.

Figure 9. Effect of pressure on the laminar flame speed obtaine with new mechanism for syngas type 1and comparison with different kinetic mechanisms.

Figure 10. Comparison of CFD in-cylinder pressure obtained using the new mechanism with the results using different chemical kinetics mechanisms for syngas types 1-3, equivalence ratio 0.48, 0.52, 0.6 and different timings of fuel micropilot injection.

Figure 11. The most sensitive reaction for modified syngas mechanism at temperature 1000K and pressures 10, 30 and 50 bar.

Figure 12. Comparison of reaction flows of carbon atoms for syngas Type 1 and Type 4 at 30 bar. Flow values are given in mol/(cm^3 sec)

Figure 13. Comparison of reaction flows of hydrogen atoms for syngas at temperature 1000 K and pressures 10, 30 and 50 bar. (A) type 1, (B) type 4. Fluxes below 1% of maximum flow have been filtered. Flow values are given in mol/(cm^3 sec)

Figure 14. Data obtained with modified mechanism for syngas type 4 with high H_2 and compared with other kinetic mechanisms. (A) Ignition delay calculated at temperatures 800-1052K, pressure 225kPa and equivalence ratio 0.6. (B) Laminar flame speed calculated at temperature 450K, pressure 225K and equivalence ratio 0.4-1.0.

Figure 15. Effect of different reaction rates of $H_2O_2+H=H_2+HO_2$ reaction on 3D CFD in-cylinder pressure during micro-pilot ignited syngas combustion.

Figure 16. Comparison of experimental and simulated in-cylinder pressures and heat release rates of dual-fuel micro-pilot ignited syngas combustion. Computed using 3D-CFD with new kinetic mechanism. (A-B) Type 1, (C-D) Type 2, (E-F) Type 3 and (G-H) Type 4. P_{IVC} = 225 kPa, T_{IVC} = 330 K.

Figure 17. Sequential images of dual-fuel micro-pilot ignited syngas combustion with new kinetics mechanisms. (A) New mechanism, Type 3, ϕ-0.6, θ_{inj}- 14^0BTDC, P_{IVC} = 225 kPa, T_{IVC} = 330 K. (B) Modified mechanism, Type 4, ϕ-0.6, θ_{inj}- 3^0BTDC, P_{IVC} = 225 kPa, T_{IVC} = 330 K.

TABLE CAPTIONS

Table 1. Engine specification and simulation conditions

Table 2. Syngas composition

Table 3. Chemical kinetics mechanism for micro pilot-ignited dual-fuel syngas combustion simulation (A units cal-cm-sec-K, E units cal/mol).

Table 4. Mixture composition of the ignition delay times experiments in the RCM from the University of Connecticut.

SUPPLIMENTARY DATA

Animation file 1. Diesel micro-pilot ignited dual-fuel combustion of syngas. Top View, Type 3, ϕ=0.6.

Animation file 2. Diesel micro-pilot ignited dual-fuel combustion of syngas. Side View, Type 3, ϕ=0.6.

Animation file 3. Diesel micro-pilot ignited dual-fuel combustion of syngas. Top View, Type 6, ϕ=0.6.

Animation file 4. Diesel micro-pilot ignited dual-fuel combustion of syngas. Side View Type 6, ϕ=0.6.

Table 1

Engine type	4-stroke, single cylinder water cooled
Bore x Stroke	96 x 108 mm
Swept volume	781.7 cm3
Compression ratio	16
Combustion system	Dual-fuel, direct injection
Combustion chamber	Shallow dish
Engine speed	1000 rpm
Intake valve closure (IVC)	135 deg. BTDC
Initial pressure at IVC	225 kPa
Initial temperature at IVC	330 K
Injection system	Common-rail
Nozzle hole x diameter	4x0.10 mm
Pilot fuel injection pressure	80 MPa
Pilot fuel injection quanity	1.2 mg/cycle
Equivalence ratio	Variable

Table 2

Click here to download high resolution image

Gas type	Composition					LHV (MJ/kg)	Source
	H_2 (%)	CO (%)	CH_4 (%)	CO_2 (%)	N_2 (%)		
Type 1	13.7	22.3	1.9	16.8	45.3	4.13	BMG
Type 2	20.0	22.3	1.9	16.8	39.0	4.99	BMG
Type 3	13.7	22.3	1.9	23.0	39.1	3.98	BMG
Type 4	56.8	5.9	29.5	2.2	5.6	38.69	COG

Table 3

Click here to download high resolution image

Skeletal syngas mechanism

	Reactions	A	n	E_A	Ref.
R1	C7H16+11O2=7CO2+8H2O	0.	0.	0.	[47]
	/EBU/ 4. 0. 1 0.				
R2	CH4+O2=CH3+HO2	3.98E13	0.0	56855.5	[46]
R3	CH4+HO2=CH3+H2O2	0.964E11	0.0	24629.4	[46]
R4	CH4+OH=CH3+H2O	1.60E07	1.83	2771.1	[73]
R5	CH3+O2=CH2O+OH	3.30E11	0.0	8934.4	[25]
R6	CH2O+OH=HCO+H2O	3.90E10	0.0	406.1	[46]
R7	CO+O(+M)=CO2(+M)	9.04E12	0.89	3800.0	[25]
	/LOW / 0.2070E27 -3.340 7610.0				
	/M/ H2O/12.00/ H2/2.00/ CO/1.50/ CO2/2.00/ AR/0.50/				
R8	CO+OH=CO2+H	0.9600E12	0.14	7352.0	[25]
R9	CO+OH=CO2+H	0.7320E11	-1.00	-16.0	[25]
R10	CO+HO2=CO2+OH	0.1200E18	0.00	17000.0	[25]
R11	CO+H2O=CO2+H2	0.2000E9	0.00	38000.0	[25]
R12	HCO(+M)=CO+H(+M)	0.3000E14	0.03	23000.0	[25]
	/M/ H2O/5.00/ CO2/3.00/ H2/1.90/ CO/1.90/				
R13	HCO+O=CO2+H	0.3000E14	0.00	0.0	[25]
R14	HCO+H=H2+CO	0.1000E13	0.00	0.0	[25]
R15	HCO+OH=H2O+CO	0.5000E14	0.00	0.0	[25]
R16	HCO+HO2=H2O2+CO	0.4000E12	0.00	0.0	[25]
R17	HCO+HO2=>H+OH+CO2	0.3000E14	0.00	0.0	[25]
R18	O2+CO=CO2+O	0.2530E10	0.00	0.0	[25]
R19	O2+HCO=HO2+CO	0.1000E15	0.00	47700.0	[25]
R20	OH+OH(+M)=H2O2(+M)	0.7400E14	-0.370	0.0	[25]
	/LOW / 0.2300E19 -0.900 -1700.0				
	/TROE/ 0.7346 94.00 1756.0 5182.0				
	/M/ H2/2.00 /H2O/6.00/ CO/1.50/ CO2/2.00/ AR/0.70/				
R21	H+O2=OH+O	3.52E16	-0.7	17061.4	[63]
R22	H2+O=OH+H	5.06E4	2.67	6287.6	[79]
R23	H2+OH=H2O+H	1.17E9	1.3	0.0	[79]
R24	H+O2(+M)=>HO2(+M)	4.6E12	0.4	0.0	[35]
	/LOW / 1.737E19 -1.23 0.0				
	/M/ AR/0.0/ H2/1.3/ H2O/10.0/ CO/1.9/ CO2/3.8/				
R25	H+H+(M)=>H2+(M)	1.30E18	-1	0.0	[63]
	/M/ H2/2.5/ H2O/12.0/ CO/1.9 /CO2/3.8/ AR/0.5/				
R26	H+OH(+M)=>H2O(+M)	4.00E22	-2	0.0	[63]
	/M/ H2/2.5/ H2O/12.0/ CO/1.9/ CO2/3.8/ AR/0.38/				
R27	HO2+H=>OH+OH	7.08E13	0.0	298.8	[97]
R28	HO2+H=H2+O2	1.66E13	0.0	821.8	[35]
R29	HO2+OH=H2O+O2	2.89E13	0.0	-500	[42]
R30	HO2+HO2=H2O2+O2	1.300E11	0.00	-1.630E03	[35]

Additional reactions for biomass feedstock derived gas (low H_2 concentration)

	Reactions	A	n	E_A	Ref.
R29b	HO2+OH=H2O+O2	2.456E13	0.0	-4.97E02	[35]
R31	H2O2+H=H2+HO2	7.7E12	0.0	3755	[42]
R32	O+H2O=OH+OH	2.97E06	2.02	1.340E04	[35]

Reaction constants for coke-oven feedstock derived gas (high H_2 concentration)

	Reactions	A	n	E_A	Ref.
R31	H2O2+H=H2+HO2	1.21E07	0.0	5200	[49]

Table 4

Click here to download high resolution image

H_2 (%)	CO (%)	O_2 (%)	N_2 (%)	T_c (K)
12.500	0.000	6.250	81.250	914 -1010
6.250	6.250	6.250	81.250	929 -1031
3.125	9.375	6.250	81.250	959 -1052
1.250	11.250	6.250	81.250	973 -1068

Figure 1

Click here to download high resolution image

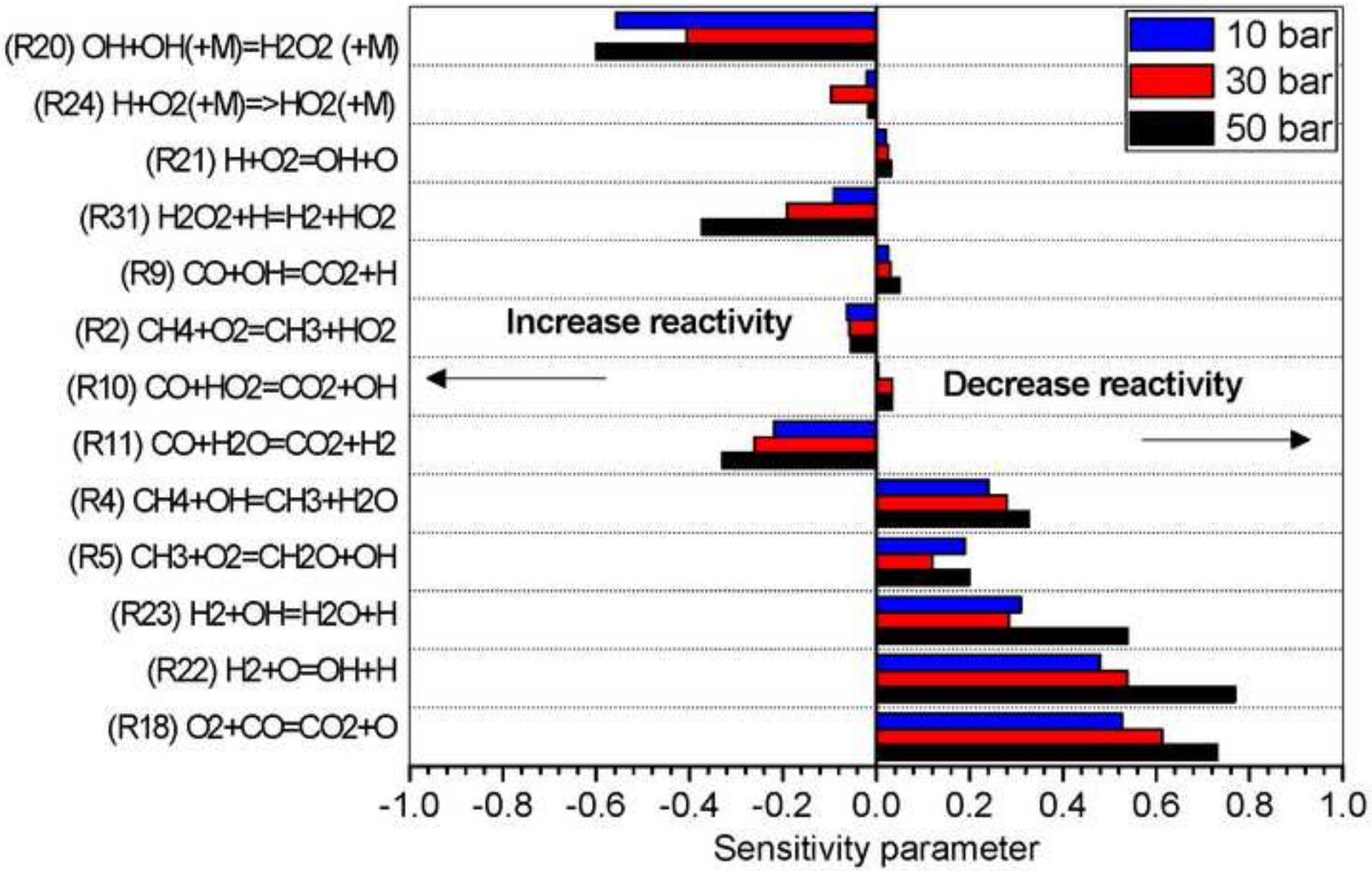

Figure 2

Click here to download high resolution image

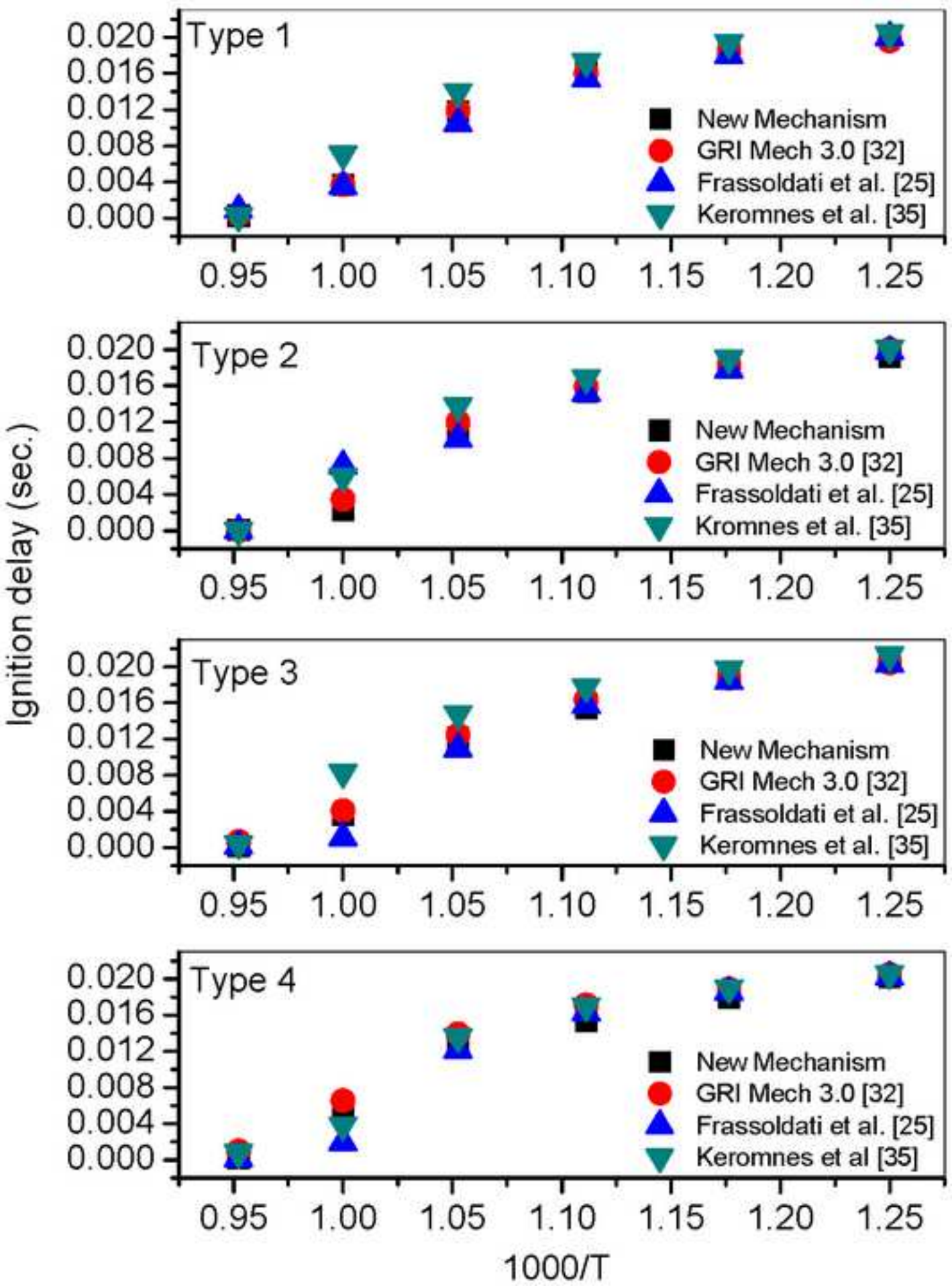

Figure 3

Click here to download high resolution image

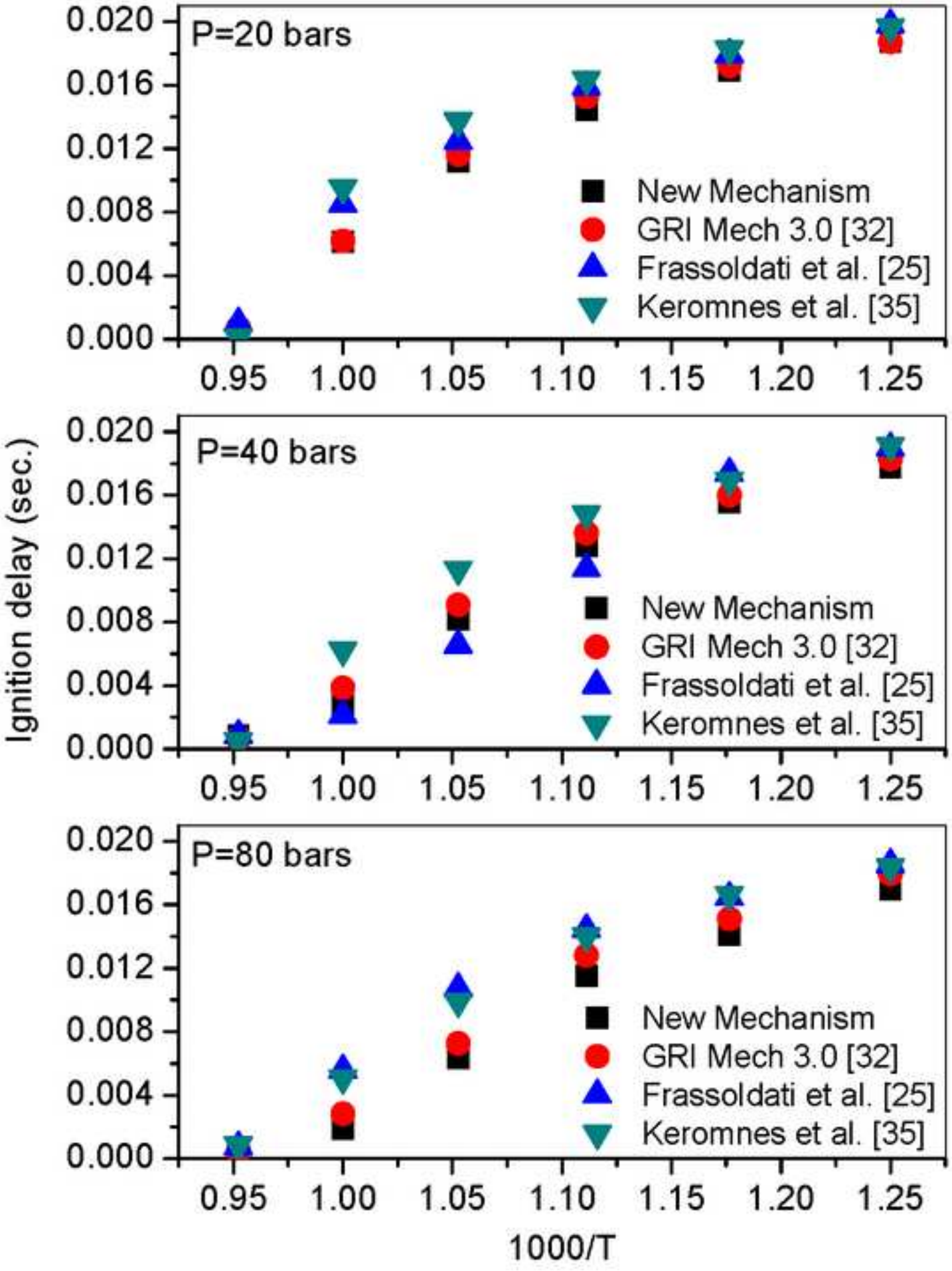

Figure 4

Click here to download high resolution image

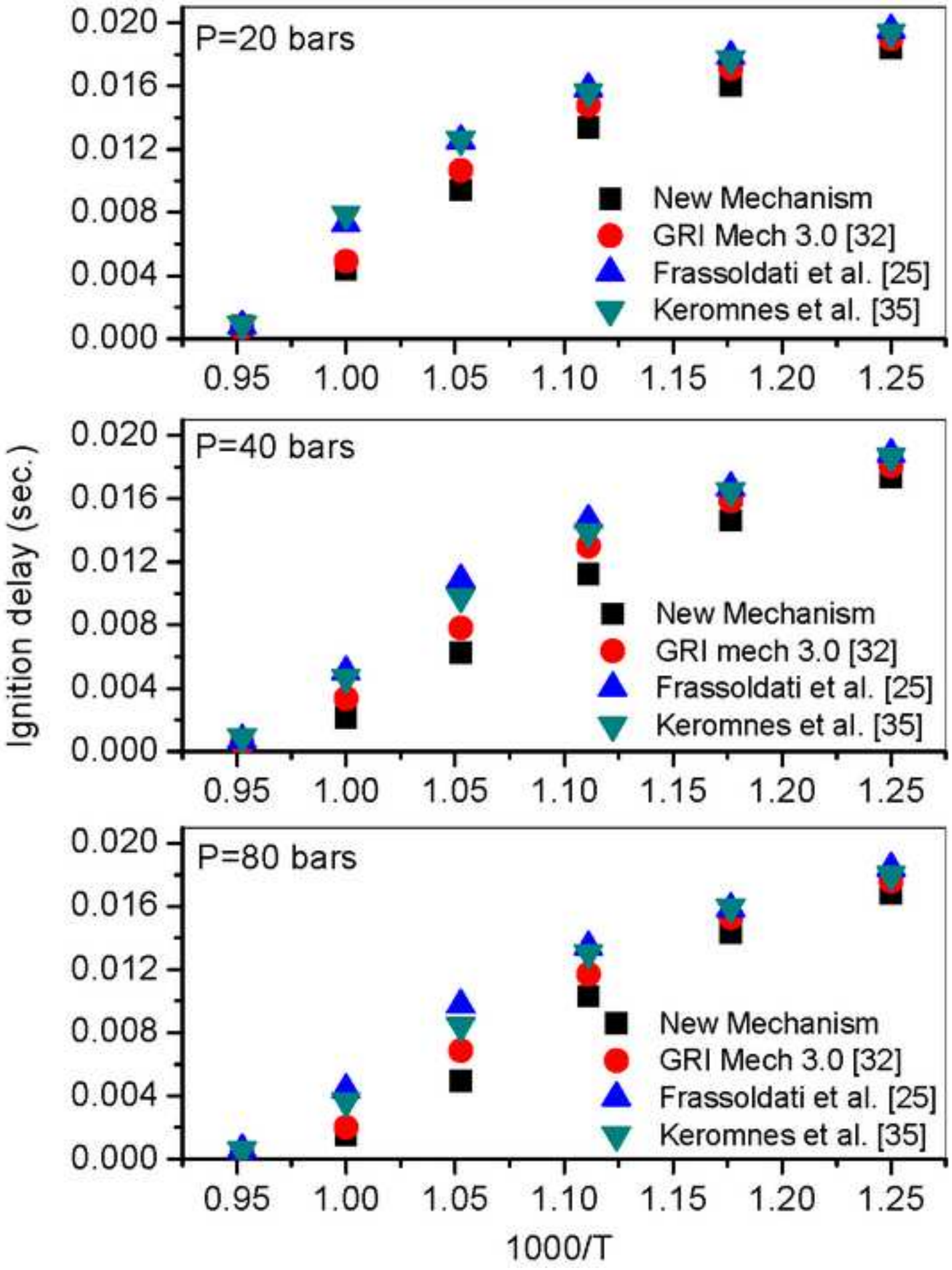

Figure 5

Click here to download high resolution image

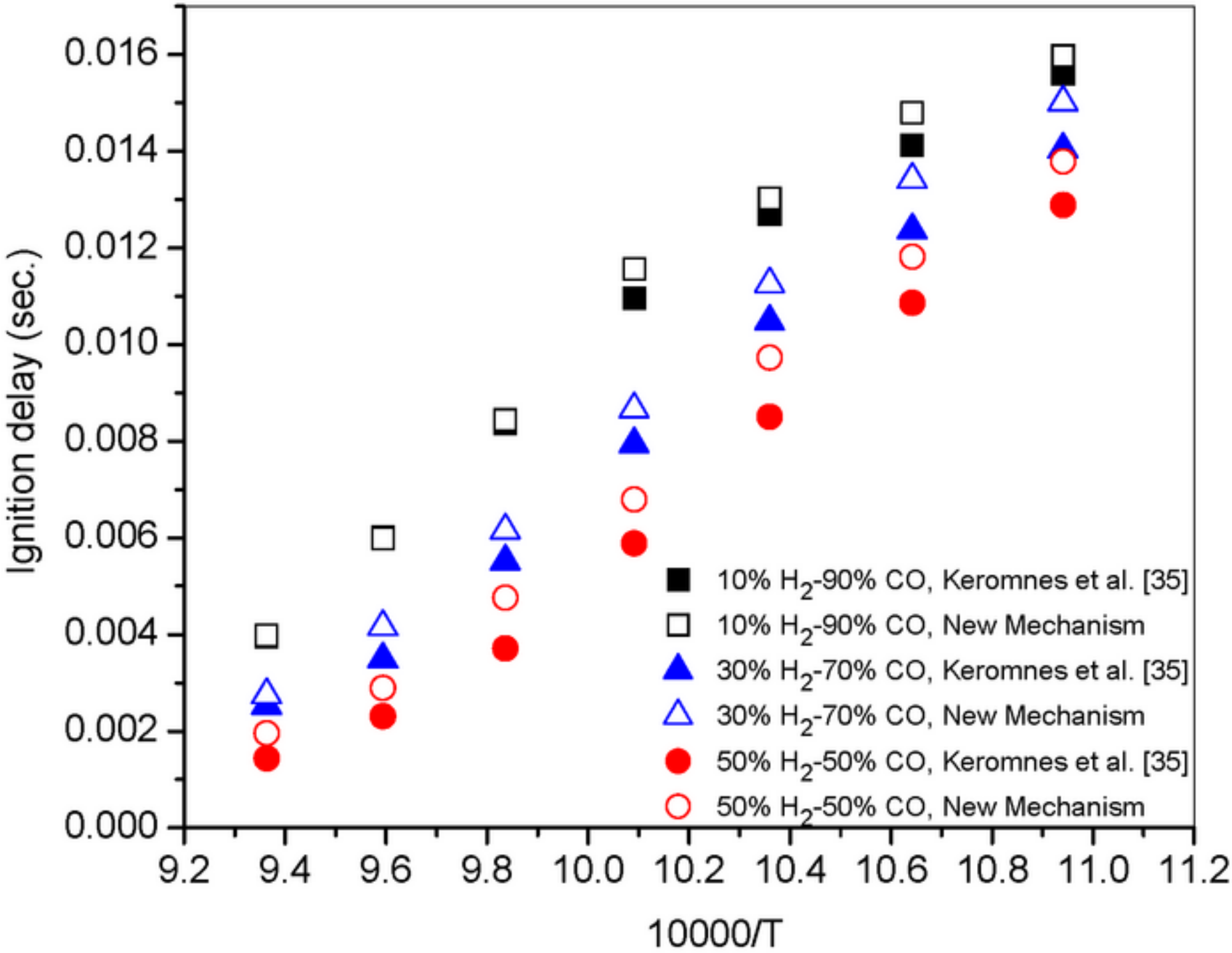

Figure 6

Click here to download high resolution image

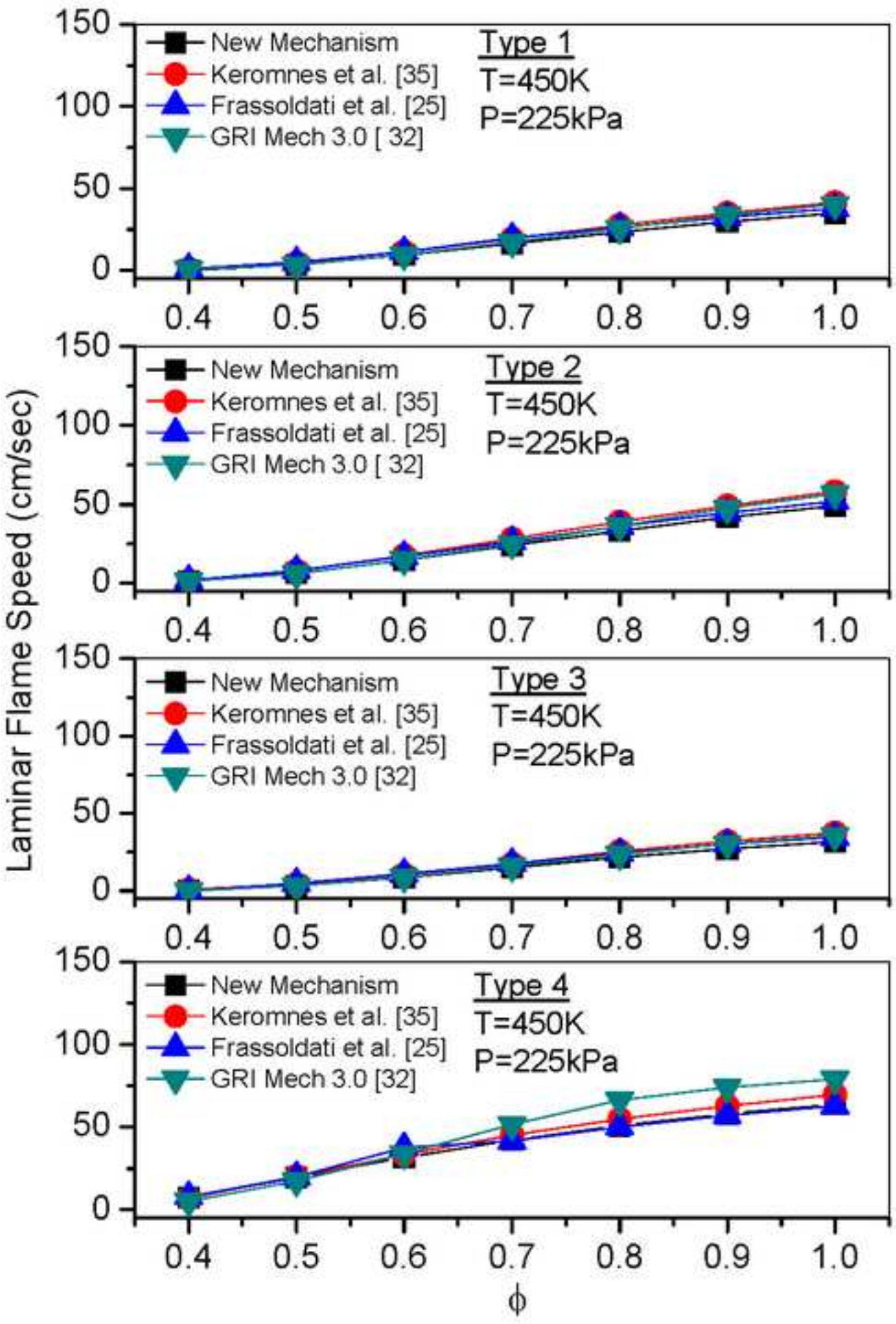

Figure 7

Click here to download high resolution image

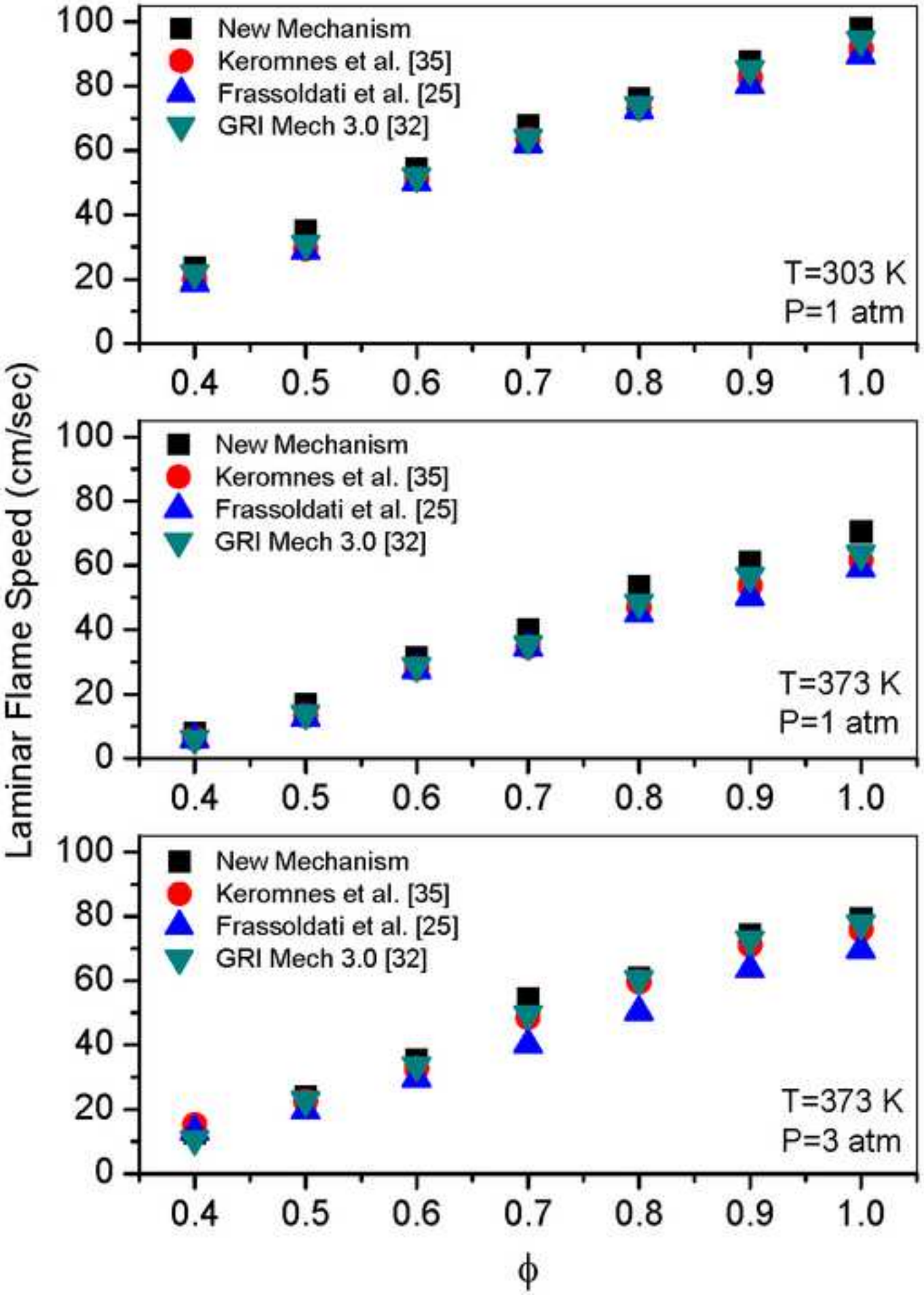

Figure 8

Click here to download high resolution image

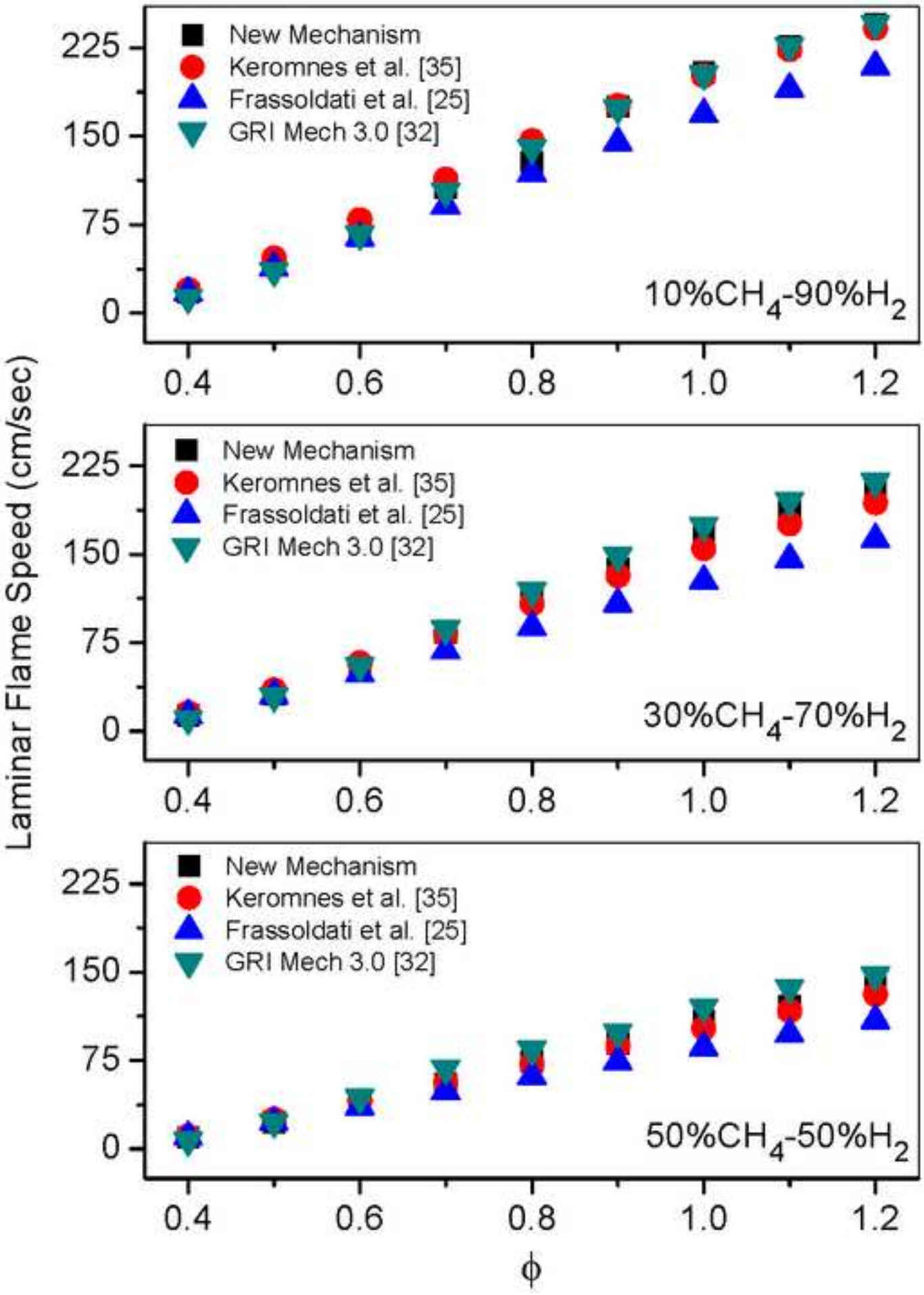

Figure 9
Click here to download high resolution image

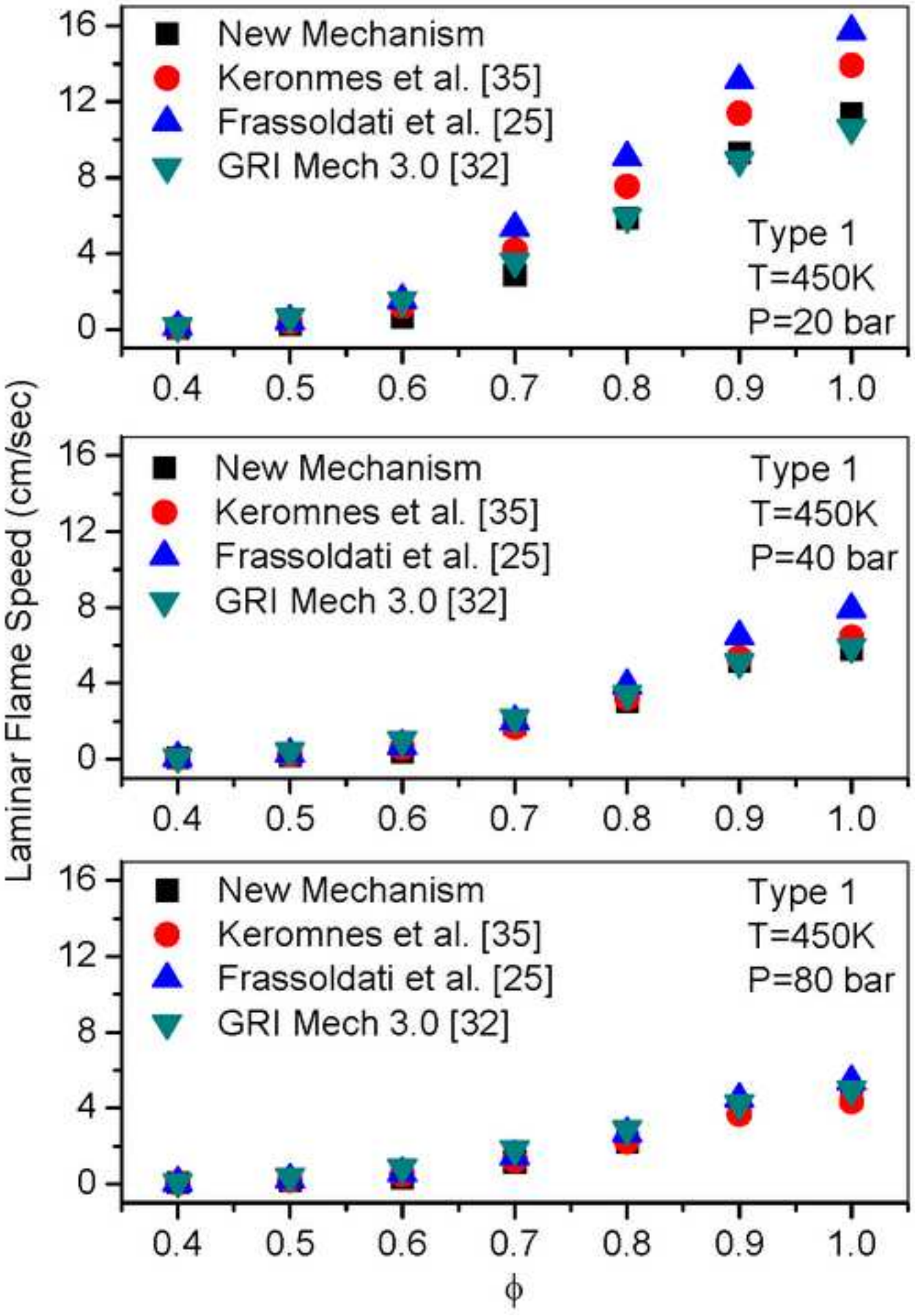

Figure 10

Click here to download high resolution image

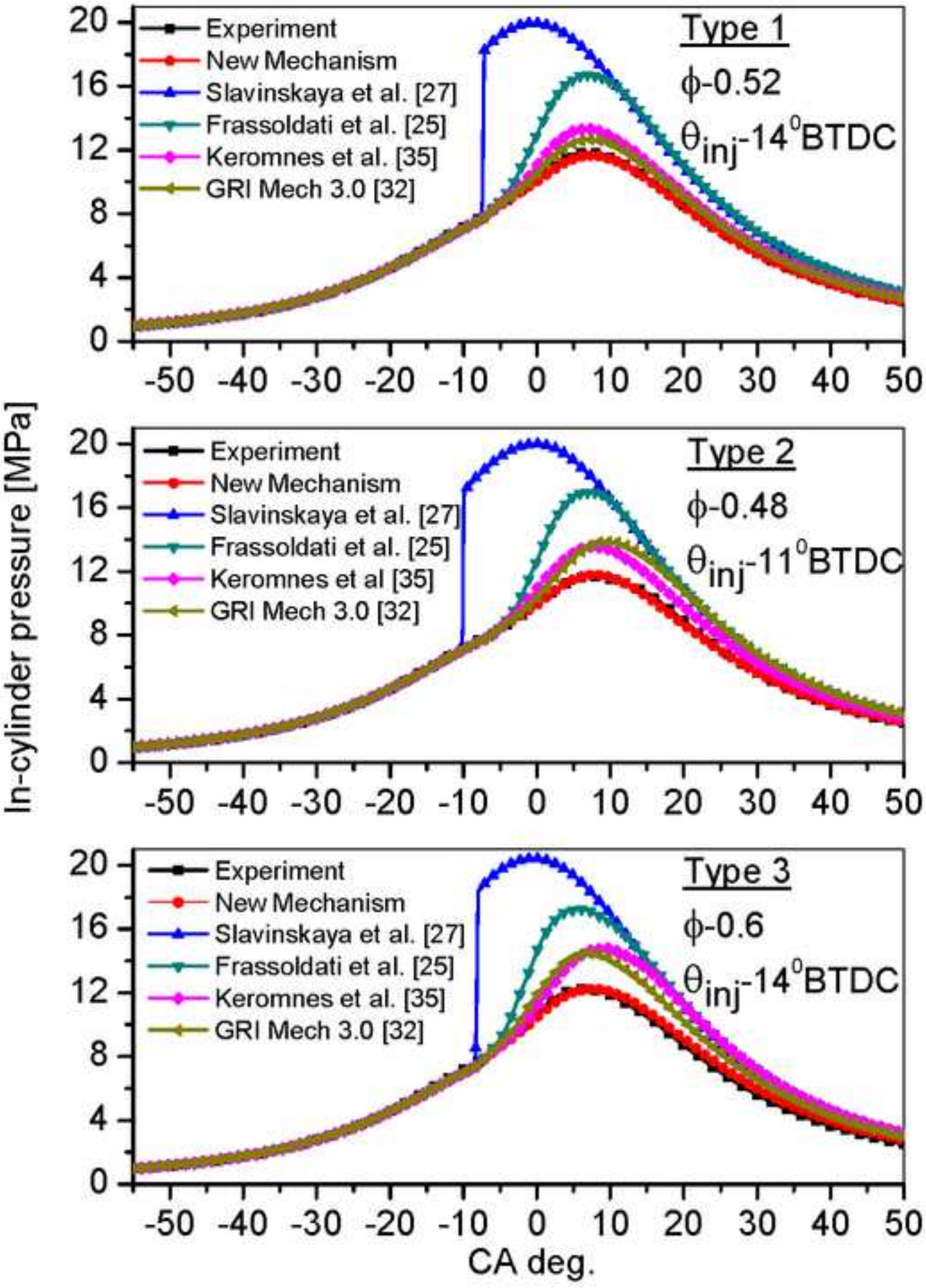

Figure 11

Click here to download high resolution image

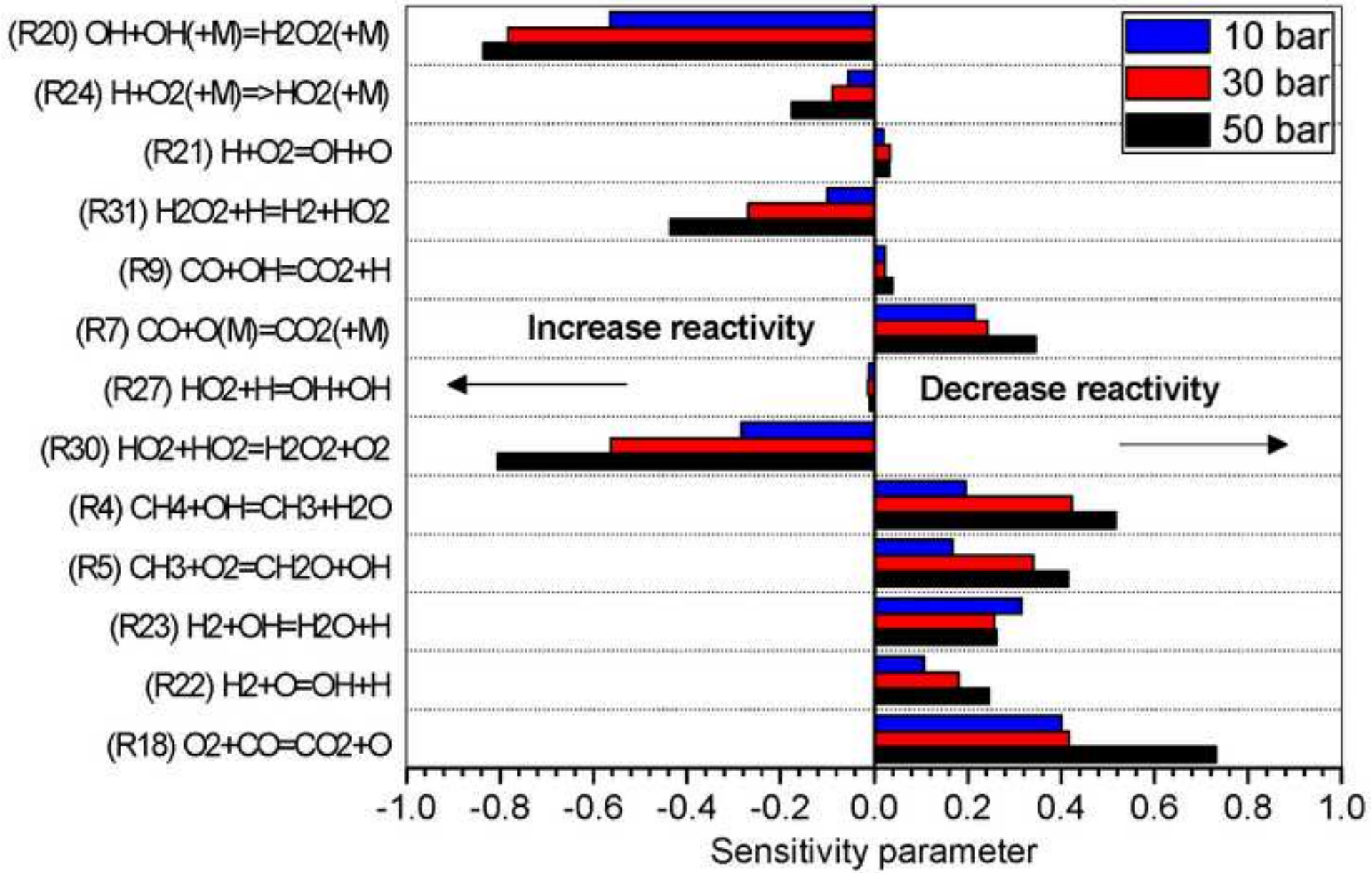

Figure 12

Click here to download high resolution image

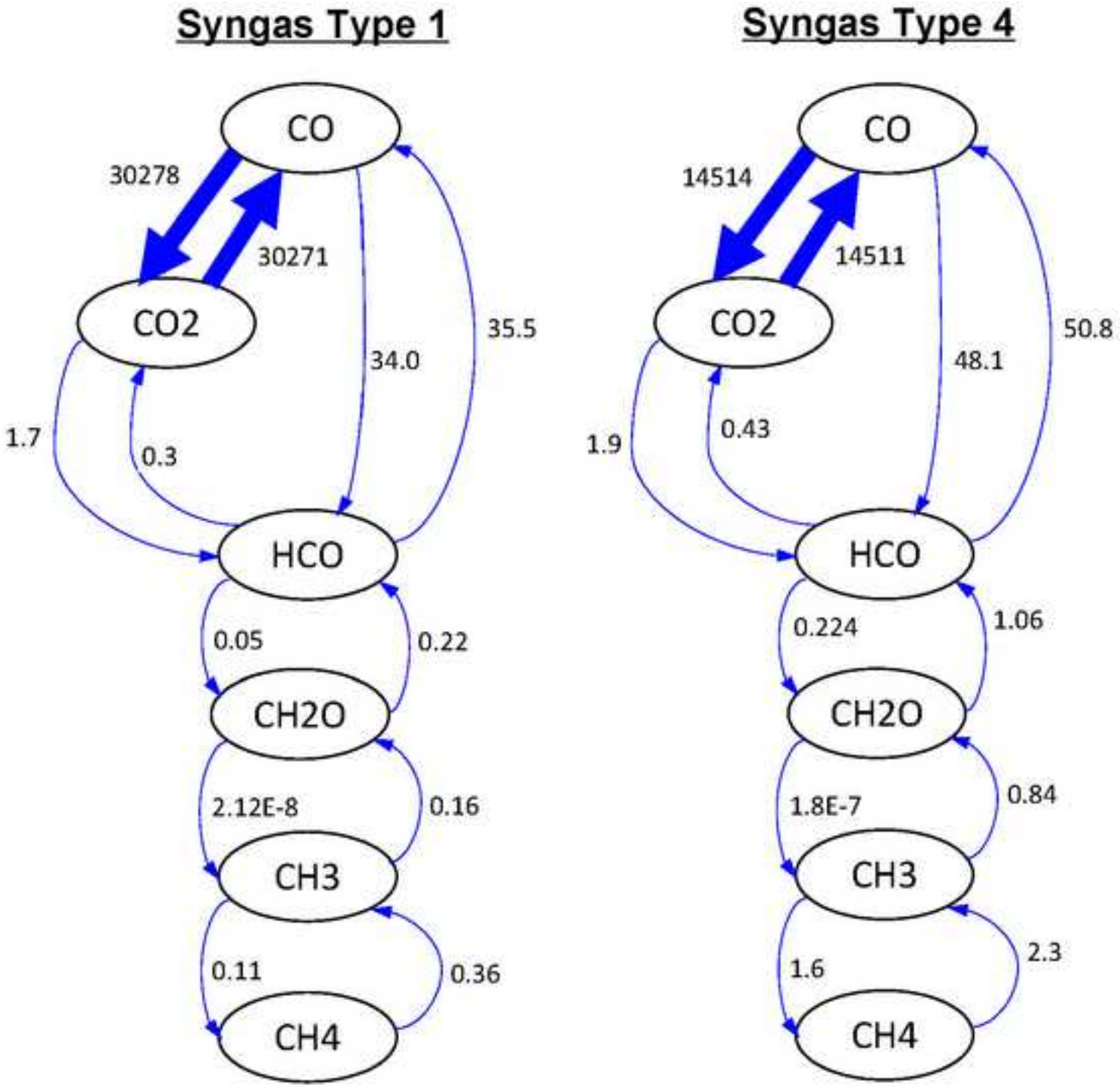

Figure 13

Click here to download high resolution image

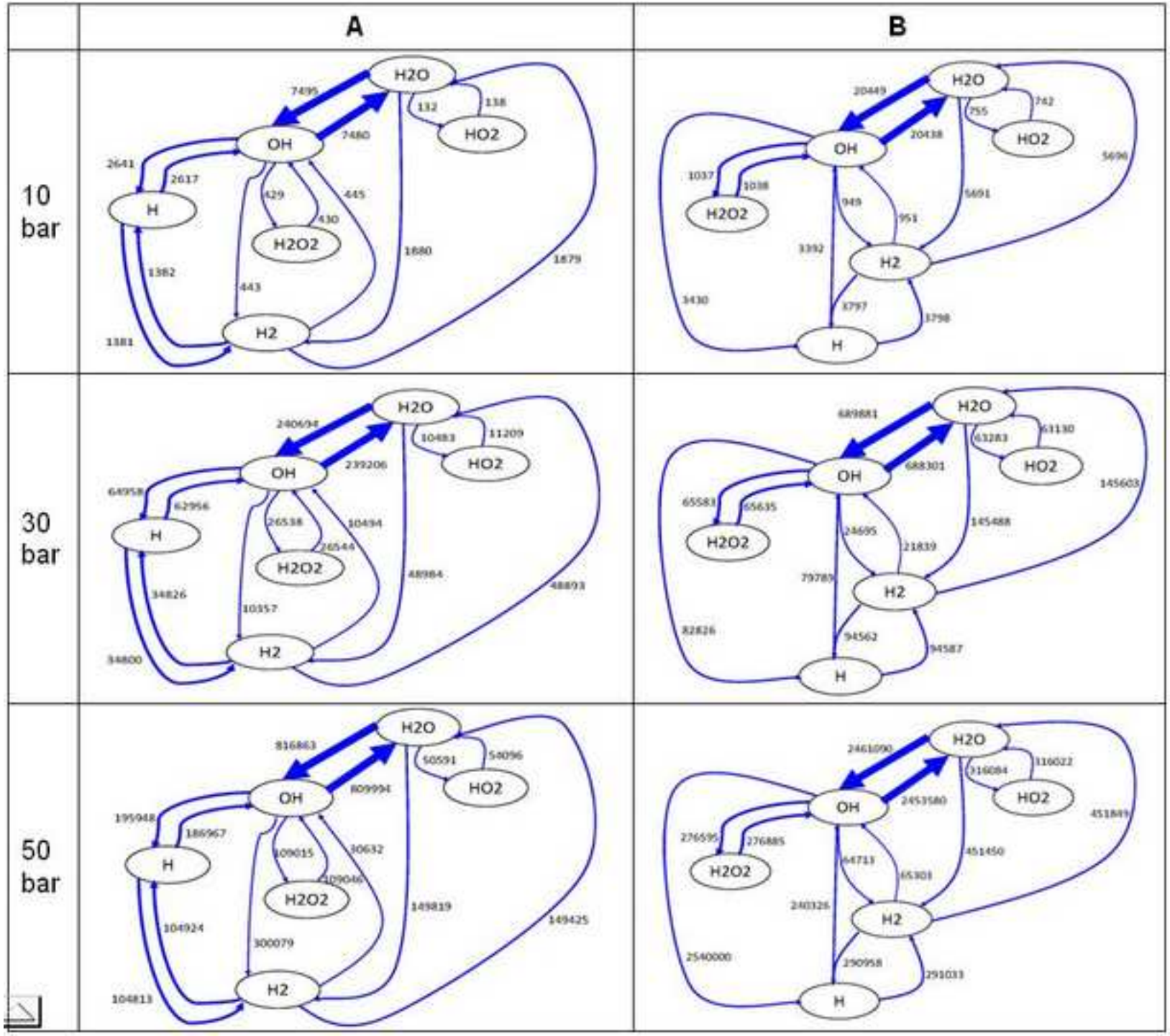

Figure 14

Click here to download high resolution image

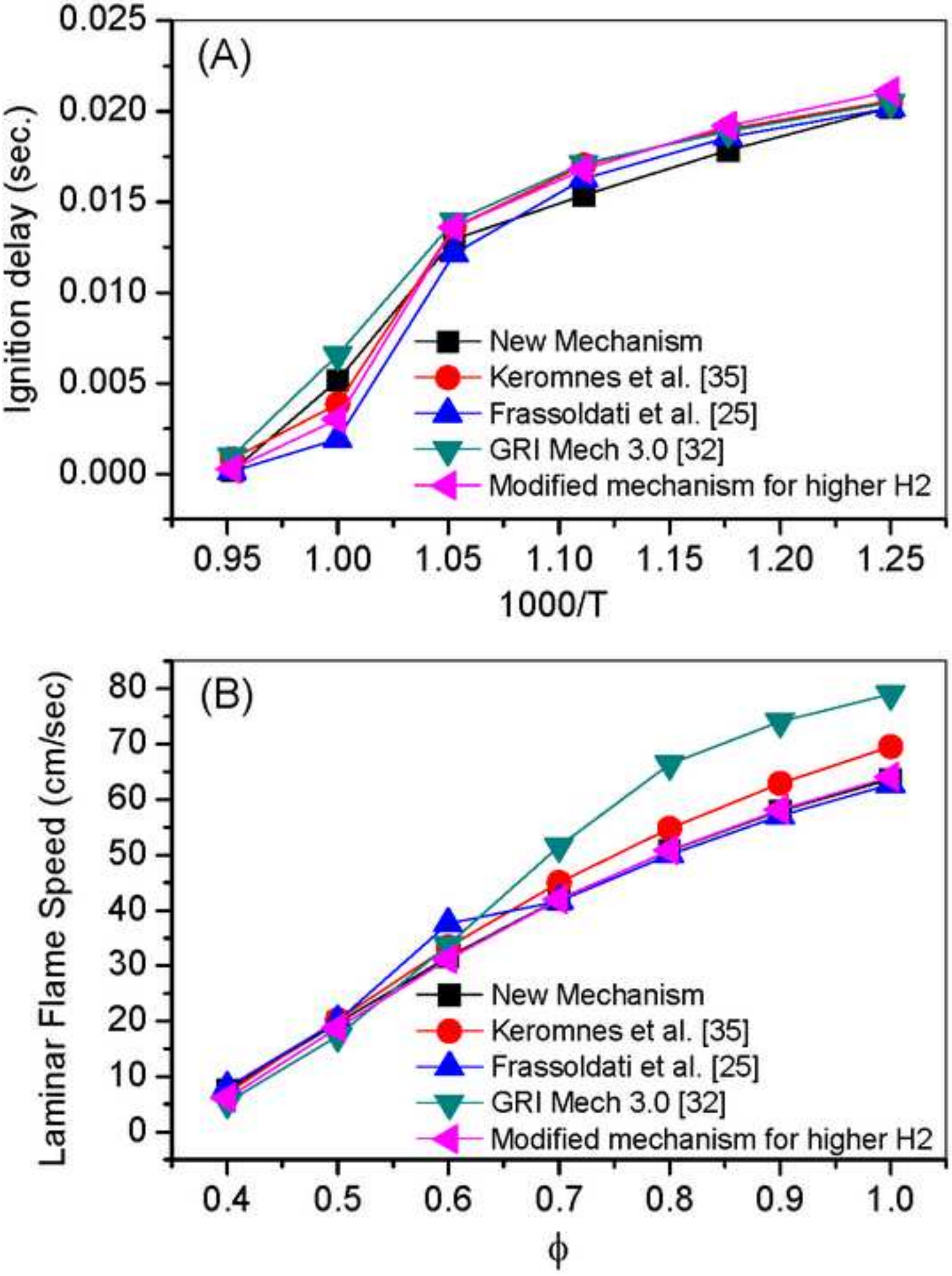

Figure 15

Click here to download high resolution image

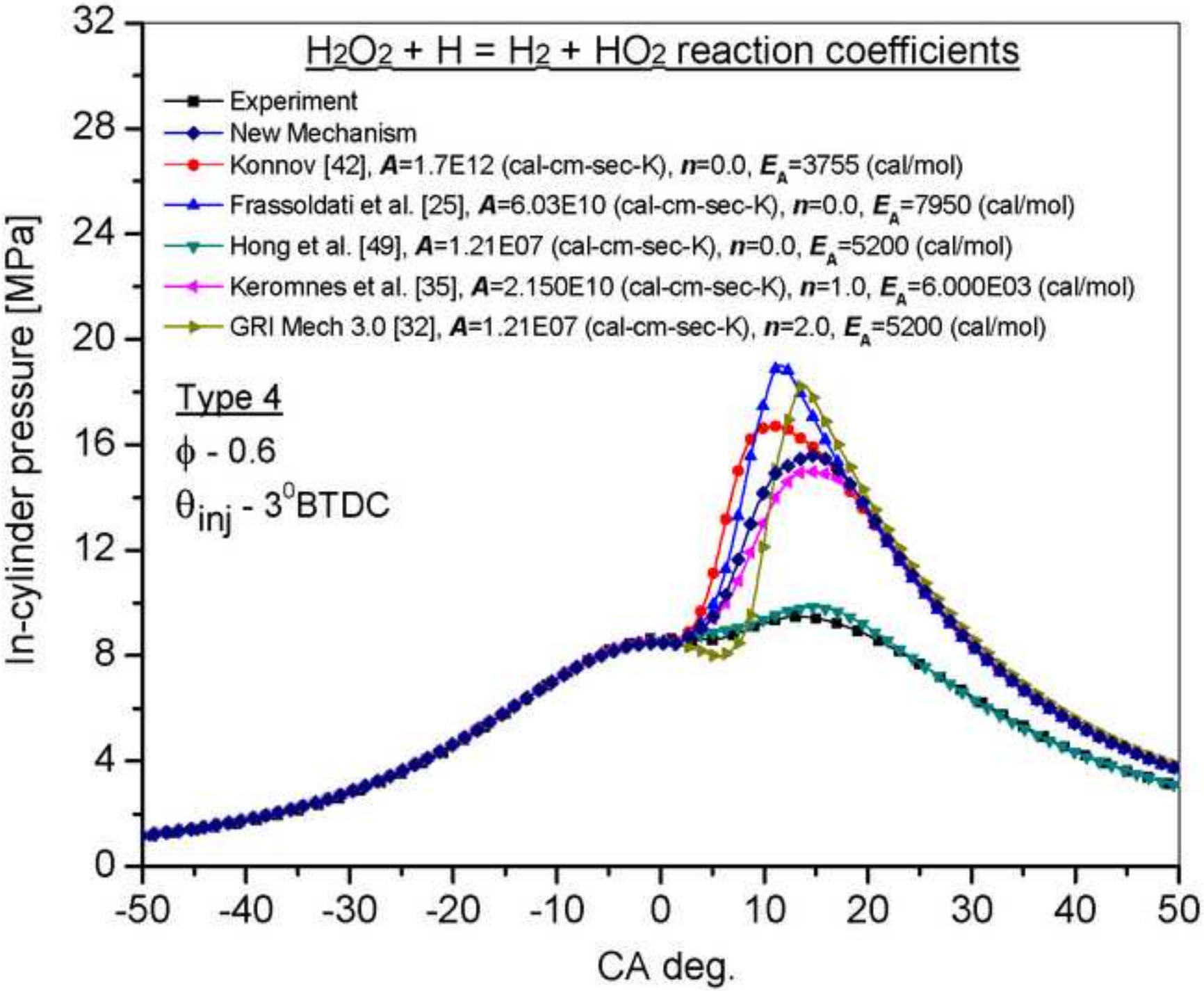

Figure 16

Click here to download high resolution image

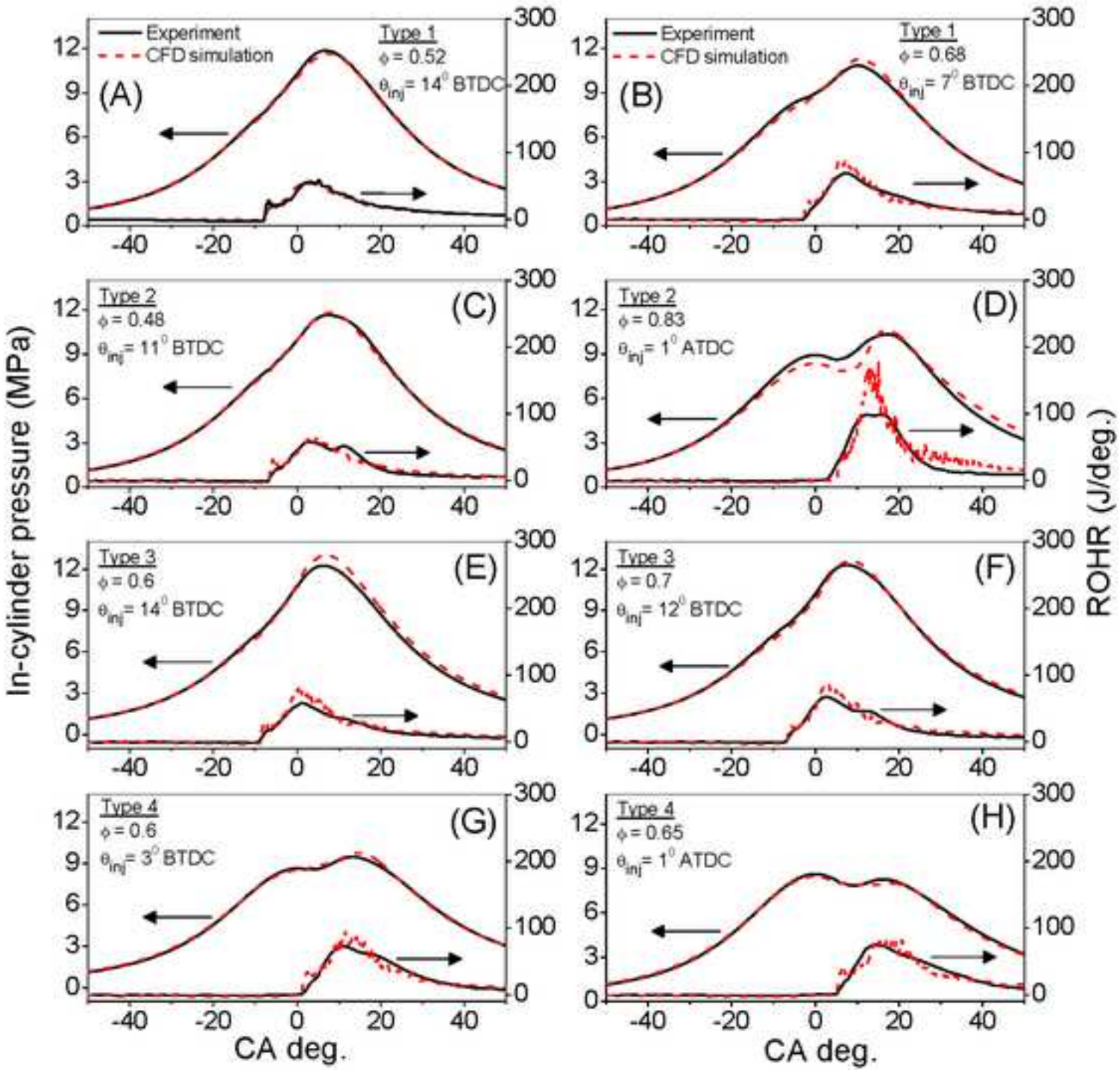

Figure 17

Click here to download high resolution image

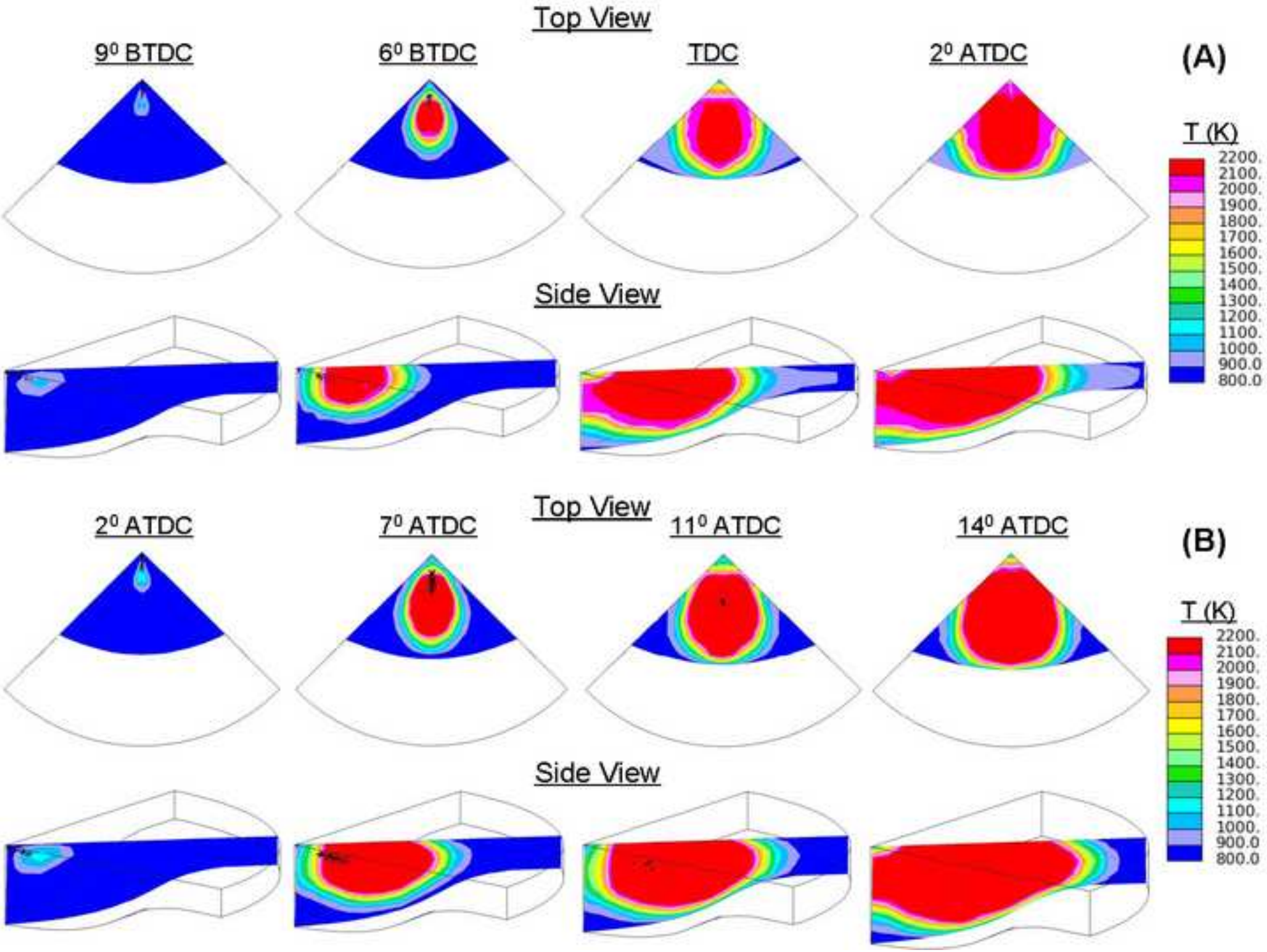

Animation File 1_Top View, Type 3_06

Click here to download Supplementary Material: Animation File 1_Top View, Type 3_06.gif

Animation File 2_Side View, Type 3_06

Click here to download Supplementary Material: Animation File 2_Side View, Type 3_06.gif

Animation File 3_Top View, Type 4_06

Click here to download Supplementary Material: Animation File 3_Top View, Type 4_06.gif

Animation File 4_Side View, Type 4_06

Click here to download Supplementary Material: Animation File 4_Side View, Type 4_06.gif

Supplementary Material

Click here to download Supplementary Material: Attachment 1.tif

Supplementary Material

Click here to download Supplementary Material: Attachment 2.tif

Supplementary Material

Click here to download Supplementary Material: Attachment 3.tif